GSK-3 modulates SHH-driven proliferation in postnatal cerebellar neurogenesis and medulloblastoma.

Jennifer K. Ocasio[1], Rolf Dale P. Bates[2], Carolyn D. Rapp[2], and Timothy R. Gershon[1,2,3]

[1]UNC Neuroscience Center, University of North Carolina, Chapel Hill, North Carolina 27599, USA
[2]Department of Neurology, UNC School of Medicine, University of North Carolina, Chapel Hill, North Carolina 27599, USA
[3]Lineberger Comprehensive Cancer Center, University of North Carolina, Chapel Hill, North Carolina 27599, USA

Corresponding authors: gershont@neurology.med.unc.edu, ocasio@email.unc.edu

Keywords: GSK-3, WNT, cerebellar development, medulloblastoma, cell cycle, postnatal neurogenesis

Summary statement: WNT signaling must be suppressed by GSK-3 to permit Sonic-hedgehog (SHH)-driven postnatal cerebellar neurogenesis and medulloblastoma tumor growth. GSK-3 may be targeted as a novel therapy for SHH-driven medulloblastoma.

Abstract:

Cerebellar development requires regulated proliferation of cerebellar granule neuron progenitors (CGNPs). Inadequate CGNP proliferation causes cerebellar hypoplasia while excessive CGNP proliferation can cause medulloblastoma, the most common malignant pediatric brain tumor. Although Sonic Hedgehog (SHH) signaling is known to activate CGNP proliferation, the mechanisms down-regulating proliferation are less defined. We investigated CGNP regulation by GSK-3, which down-regulates proliferation in the forebrain, gut and breast by suppressing mitogenic WNT signaling. In striking contrast, we found that co-deleting *Gsk-3α* and *Gsk-3β* blocked CGNP proliferation, causing severe cerebellar hypoplasia. The GSK-3 inhibitor CHIR-98014 similarly down-regulated SHH-driven proliferation. Transcriptomic analysis showed activated WNT signaling and up-regulated *Cdkn1a* in *Gsk-3*-deleted CGNPs. *Ctnnb* co-deletion increased CGNP proliferation and rescued cerebellar hypo-proliferation in *Gsk-3α/β* mutants, demonstrating physiologic control of CGNPs by GSK-3, mediated through WNT. SHH-driven medulloblastomas similarly required GSK-3, as co-deleting *Gsk-3α/β* blocked tumor growth in medulloblastoma-prone *SmoM2* mice. These data show that a GSK-3/WNT axis modulates the developmental proliferation of CGNPs and the pathologic growth of SHH-driven medulloblastoma. The requirement for GSK-3 in SHH-driven proliferation suggests that GSK-3 may be targeted for SHH-driven medulloblastoma therapy.

Introduction

Strict control of progenitor proliferation and differentiation are required for brain growth. Inadequate proliferation causes microcephaly while excessive proliferation may support tumorigenesis (Chizhikov and Millen, 2003; Grimmer and Weiss, 2006; Yang et al., 2009; Garel et al., 2011; Lang and Gershon, 2018). Cerebellar growth depends on the proliferation of CGNPs, which continues into postnatal life (Ten Donkelaar and Lammens, 2009; Marzban et al., 2015). CGNPs proliferate rapidly in response to Sonic hedgehog (SHH) signaling to give rise to the largest population of neurons in the brain (Wechsler-Reya and Scott, 1999). Disruptions in regulation of CGNP proliferation can give rise to severe neurological disorders including cerebellar hypoplasia and medulloblastoma (Ten Donkelaar and Lammens, 2009; Roussel and Hatten, 2011). While medulloblastomas are typically responsive to a combination of surgery, radiation and chemotherapy, this treatment causes long-term adverse effects and fails 10-20% of patients (Polkinghorn and Tarbell, 2007; Northcott et al., 2012). Understanding the mechanisms that regulate SHH-driven proliferation may lead to new insight into the pathogenesis of both cerebellar hypoplasia and tumorigenesis, and may lead to novel therapeutic approaches to medulloblastoma.

We examined the regulation of CGNPs and SHH-driven medulloblastoma by glycogen synthase kinase (GSK-3), which has been shown to down-regulate proliferation in multiple cellular contexts. GSK-3 is a serine-threonine kinase that acts on the intracellular transducers of diverse signaling pathways, including WNT and SHH (Cole, 2012; Bengoa-Vergniory and Kypta, 2015). The mammalian genome includes two GSK-3 isozymes, *Gsk-3α* and *Gsk-3β*, which are encoded by distinct loci. In a study of mouse forebrain neural progenitors, co-deletion of *Gsk-3α* and *Gsk-3β* caused hyper-proliferation and delayed neuronal differentiation (Kim et al., 2009; Morgan-Smith et al., 2014). A similar phenotype was seen with deletion of *Gsk-3α* and *Gsk-3β* in breast epithelial cells (Zhao et al., 2014), where β-catenin (CTNNB) mediated this mitogenic effect.

The growth suppressive role of GSK-3 in the embryonic forebrain and in gut and breast epithelia suggest a role for GSK-3 in down-regulating proliferation. This possibility is supported by studies showing that GSK-3 destabilizes MYCN, a required effector of mitogenic SHH signaling (Knoepfler and Kenney, 2006). However, an alternative possibility is suggested by the pattern of WNT and SHH pathway activation in medulloblastoma.

Transcriptomic studies of medulloblastomas resected from patients have defined subsets of tumors with activation of either WNT or SHH. However, no subset shows up-regulation of both WNT and SHH. While both SHH (Wechsler-Reya and Scott, 1999; Kenney and Rowitch, 2002) and WNT signaling (Harada et al., 1999; Jho et al., 2002; Zechner et al., 2003; Akiyoshi et al., 2006) are known to support proliferation in diverse cell types, the absence of medulloblastomas with simultaneous activation of WNT and SHH suggests that in specific cells of origin, these two pathways may not have additive oncogenic effects. Consistent with this possibility, SHH activation and WNT activation recapitulate medulloblastomas from distinctly different pre-malignant cells that derive from different regions of the rhombic lip (Schüller et al., 2008; Gibson et al., 2010; Vladoiu et al., 2019). In other cellular contexts, moreover, the WNT and SHH pathways are antagonistic. For example, endogenous WNT activation inhibits SHH signaling in hES cells and in the dorsal neural tube (Li et al., 2009; Ulloa and Martí, 2010), and exogenous activation of WNT through forced expression of a constitutively active allele of CTNNB has been shown to reduce both SHH-driven CGNP proliferation and medulloblastoma growth (Schuller and Rowitch, 2007; Pöschl et al., 2013; Pöschl et al., 2014). The inhibitory effect of CTNNB on SHH-driven proliferation raises the possibility that GSK-3, which targets CTNNB for degradation, may be growth-permissive, rather than growth-suppressive. Studies using LiCl, which inhibits GSK-3 activity, have provided evidence to support this possibility (Sato et al., 2004; Yeste-Velasco et al., 2007; Zinke et al., 2015).

To resolve definitively whether and how GSK-3 exerts physiologic modulation of SHH-driven proliferation in CGNPs and medulloblastoma, we analyzed *Gsk-3α* null mice with conditional deletion of *Gsk-3β* in CGNPs. We found that deletion of both *Gsk-3* loci caused profound cerebellar hypoplasia due to impaired CGNP proliferation. Deletion of both *Gsk-3* loci also blocked medulloblastoma growth in mice expressing *SmoM2*, a constitutively active allele of *Smo* that typically induces SHH-driven medulloblastoma with 100% penetrance. These findings show that GSK-3 can exert a diametrically opposite effect on growth that depends on the cellular context, and define a previously unknown role for GSK-3 regulation of cerebellar development that is preserved in SHH-driven medulloblastoma.

Results

Gsk-3 deletion induces severe cerebellar hypoplasia

To investigate GSK-3 function in CGNPs, we bred *Gsk-3α*$^{-/-}$ and *Math1-Cre/Gsk-3β*$^{loxP/loxP}$ mice. Within the cerebellum, the MATH1 lineage includes the CGNPs and the neurons of the deep cerebellar nuclei (Wang et al., 2005). CGNPs in *Math1-Cre* mice undergo recombination at LoxP sites beginning from E12.5, in a rostro-caudal progression from the anterior to posterior regions of the cerebellar cortex (Machold and Fishell, 2005; Wang et al., 2005). We did not detect phenotypic changes in either the *Gsk-3α*$^{-/-}$ or *Math1-Cre/Gsk-3β*$^{loxP/loxP}$ genotypes. However, crossing these genotypes to generate *Math1-Cre/Gsk-3α*$^{-/-}$*/Gsk-3β*$^{loxP/loxP}$ (*Gsk-3*^{DKO}) mice resulted in severe cerebellar growth failure (Fig. 1A, P21), demonstrating that GSK-3 is required for cerebellar development, and that either *Gsk-3α* or *Gsk-3β* can meet this requirement.

Gsk-3^{DKO} mice were born with expected Mendelian frequency. The pups were viable in the neonatal period but by postnatal day 12 (P12) exhibited severe tremors, were unable to be weaned at P20-22, and did not survive beyond this age. *Gsk-3*^{DKO} mice were born with normal cerebellar architecture, with CGNPs arrayed in an external granule layer (EGL) along the outside of the primordial cerebellum, as expected (Fig. 1A, P0). By P3, however, the EGL was markedly thinned and cerebellar foliation was markedly reduced, indicating that the CGNP population did not expand appropriately from P1-P3 in *Gsk-3*^{DKO} mice (Fig. 1A, P3). The differentiated progeny of CGNPs, the cerebellar granule neurons (CGNs) of the internal granule layer (IGL) were also markedly reduced. While the IGL became progressively more densely populated in control cerebella from P1-P7, no accumulating population was readily discernible in this region in the *Gsk-3*^{DKO} mice (Fig. 1A, P2-21). The absence of an IGL demonstrated the failure of *Gsk-3*^{DKO} CGNPs to generate an appropriately large population of neurons.

The alteration of CGNP development in the *Gsk-3*^{DKO} mice disrupted the process of cerebellar foliation. However, in the P2 cerebellum where the phenotype of the *Gsk-3*^{DKO} becomes discernable, other cell types, including Bergmann glia and Purkinje neurons approximated their normal positioning along the internal margin of the EGL (Fig. S1). The radial processes of the Bergmann glia extend into the EGL of both control and *Gsk-3*^{DKO} cerebella. The relative preservation of these cell types is expected, because they are outside the *Math1* lineage and do not undergo *Gsk-3* deletion. However, it is possible that non-cell autonomous effects alter these cells in ways that we do not detect.

GSK-3 is required for CGNPs to maintain a proliferative state

We examined whether the severe hypoplastic phenotype seen in *Gsk-3*^{DKO} was caused by decreased proliferation or increased apoptosis. We compared apoptosis in *Gsk-3*^{DKO} and control cerebella either at P2, before the onset of hypoplasia, and at P3, using immunohistochemical detection of the apoptotic marker cleaved Caspase-3 (cC3). We did not detect a significant increase in apoptosis at either time point (Fig. 1B,C). In contrast, we readily found cC3^{+} cells in cerebella of *Math1-Cre/Atr*$^{loxP/loxP}$ (*Atr*^{cKO}) mice, which we have shown to have extensive CGNP apoptosis (Lang et al., 2016) providing a positive control for cC3 detection. To evaluate the possibility of Caspase-independent cell death, we also compared TUNEL staining at each time point and again did not detect increased cell death in *Gsk-3*^{DKO} cerebella (data not shown).

While we did not find increased apoptosis in the *Gsk-3*^{DKO} EGL, we found a trend toward decreased expression of the proliferation marker PCNA at P2 and P3 (Fig. 1D,E). We also noted patches of increased differentiation in the *Gsk-3*^{DKO} EGL at P2, marked by expression of the differentiation marker CDKN1B (aka p27). These changes suggested the possibility of premature CGNP cell cycle exit. Examination of RB phosphorylation supported increased cell cycle exit, as we found markedly reduced populations of cells expressing phosphorylated RB (p-RB; Fig. 1F,G) in the *Gsk-3*^{DKO} EGL.

We directly compared cell cycle exit in *Gsk-3*^{DKO} and control CGNPs by *in vivo* pulse-labeling with the DNA base analogs, BrdU and EdU. We administered BrdU intraperitoneally (IP) at P1 or P2, then administered EdU IP 24 hours later, and then harvested brains 2 hours after EdU administration. Brains were fixed, embedded, and sectioned in the sagittal plane. We identified CGNPs by their position in the EGL and defined the cell cycle exit fraction as the proportion of CGNPs that were labelled by BrdU at P2 but not labelled by EdU at P3. Both the BrdU^{+} and EdU^{+} fractions of CGNPs were significantly decreased in the EGL of *Gsk-3*^{DKO} mice compared to controls, confirming reduced CGNP proliferation at P2 and P3 (Fig. 2A,B). Moreover, the cell cycle exit fraction was significantly increased in *Gsk-3*^{DKO} CGNPs (Fig. 2C),

indicating that the CGNPs that were proliferating in these mice at P2 showed reduced self-renewal relative to CGNPs in the P2 controls.

GSK-3 inhibition reproduces the growth suppressive effect of *Gsk-3α/β* co-deletion

We used the GSK-3 inhibitor CHIR-98014 (CHIR98) to determine whether a physiologically achievable reduction in GSK-3 activity, like genetic co-deletion of *Gsk-3α* and *Gsk-3β*, could reduce SHH-driven CGNP proliferation. We cultured freshly explanted CGNPs for 24 hours in media with or without SHH, or with SHH plus increasing doses of CHIR98. We then lysed cells and using western blot, quantified phosphorylated CTNNB (p-CTNNB) as a measure of GSK-3 inhibition, p-RB as a measure of proliferation, CDKN1A as a measure of cell cycle arrest, and cC3 as a measure of apoptosis (Fig. 3A). We found that CHIR98 produced dose-dependent reductions of both p-CTNNB and p-RB, reducing p-RB in SHH-treated CGNPs as effectively as SHH deprivation (Fig. 3B). GSK-3 inhibition through CHIR98 increased CDKN1A protein levels in CGNPs as compared to controls (Fig. 3B). The decrease in proliferation was not accompanied by increased apoptosis, as CHIR98 did not induce a significant or dose-related increase in cC3 (Fig. 3B). In parallel cellular quantifications, we found that CHIR98 reduced the number cells showing p-RB expression, EdU incorporation, and p-HH3 expression, demonstrating fewer cells at both S-phase and M-phase, respectively (Fig. 3C,D). Treatment of CGNPs with the GSK-3 inhibitors LY2090314 (LY209), AZD1080, or LiCl did not decrease p-RB or p-HH3 levels or reduce EdU incorporation as effectively as CHIR98 at similar concentrations (Fig. S2). These results show that modulation of SHH-driven proliferation by GSK-3 is seen outside of the context of genetic deletion and can be achieved within the dynamic range of physiological GSK-3 activity.

Transcriptional analysis of *Gsk-3* deletion implicates WNT signaling

To identify the transcriptomic changes set in motion by *Gsk-3α/β* co-deletion, we subjected *Gsk-3*^{DKO} cerebella to expression microarray analysis. We compared whole cerebella of *Gsk-3*^{DKO} mice at P1, before the onset of severe hypoplasia, to two different, age-matched control groups, *M-Cre/Gsk-3α*$^{+/-}$*/Gsk-3β*$^{loxP/loxP}$, which retain a single *Gsk-3α* allele but have no *Gsk-3β* alleles in CGNPs, and *No Cre/Gsk-3α*$^{+/-}$*/Gsk-3β*$^{loxP/+}$, which retain a single *Gsk-3α* allele and retain two *Gsk-3β* alleles in CGNPs. We identified 68 genes that were differentially expressed in the *Gsk-3*^{DKO} cerebella compared to both controls, with false discovery rate (FDR) adjusted p-value (q-value) less than 0.05 and absolute fold change (|FC|) greater than or equal to 2. 14 genes were decreased in the *Gsk-3*^{DKO} and 54 genes were increased (Fig. 4A, Table S1). Among the 14 decreased genes, we noted *Gsk-3α*, consistent

with the genetic disruption, and 3 neuronal markers, *Chrna3*, *Chrnb4*, and *Cadps2*, consistent with the reduced neuronal population of *Gsk-3*^{DKO} cerebella.

We used Gene Set Enrichment Analysis (GSEA) to define biological pathways implicated in the *Gsk-3*^{DKO} phenotype by the differential pattern of gene expression. GSEA identified the WNT and p53 pathways as activated, with up-regulation of WNT markers including *Tcf7*, *Lef1*, *Wif1*, and *Wnt10a* (Enrichment score=0.5224; q-value=0.037), and upregulation of p53 markers *Pmaip1*, *Gadd45a*, and *Cdkn1a* (Enrichment score=0.7996; q-value=0.034) (Fig. 4B,C). Immunohistochemistry confirmed increased expression of CDKN1A and LEF1 proteins in *Gsk-3*^{DKO} CGNPs identified by morphology, position in the EGL (Fig. 4D,E). To confirm the identity of LEF1 expressing cells as CGNPs, we used MATH1 (aka ATOH1) immunofluorescence to identify the proliferative CGNP population in LEF1 co-stained sections (Fig. 4E). These double label studies show absence of LEF1 in control CGNPs, and expression of LEF1 in *Gsk-3*^{DKO} cerebella in a band that includes the MATH1^{+} CGNPs and adjacent, radially inward cells that we interpret to be the differentiating CGNP population. In both the *Gsk-3*^{DKO} and controls, TCF7 was localized to cells outside the CGNP population, identified by their morphology and expression of FABP7 as Bergmann glia (Fig. 4F). The cellular distributions of LEF1, CDKN1A and TCF7 show that disrupting GSK-3 in CGNPs caused both cell autonomous and non-cell autonomous WNT activation, and cell autonomous, CGNP-specific induction of CDKN1A. To resolve the roles of WNT activation, p53, and CDKN1A in the pathogenesis of the *GSK-3*^{DKO} phenotype, we performed a series of co-deletion experiments.

Ctnnb **deletion increases CGNP proliferation and rescues the growth suppressive effect of** ***Gsk-3*** **deletion**

GSK-3 negatively regulates WNT/β-catenin signaling by phosphorylating CTNNB, which promotes its proteasomal degradation (Hagen and Vidal-Puig, 2002). To determine if CTNNB is required for the developmental regulation of SHH-driven CGNPs, we bred mice with conditional alleles of *Ctnnb* (*Ctnnb*$^{loxP/loxP}$) with *Math1-Cre* mice to generate *Math1-Cre/Ctnnb*$^{loxP/loxP}$ (*Ctnnb*^{cKO}) animals with *Ctnnb* deletion in the CGNP population. At P7, *Ctnnb*^{cKO} mice showed foci of hyperproliferation in the EGL, marked by increased thickness of the PCNA^{+} and p-RB^{+} domains of the EGL (Fig. 5A). This hyperproliferation did not lead to tumor formation, and by P15, all CGNPs in *Ctnnb*^{cKO} mice had exited the cell cycle and migrated to the IGL, as in *Ctnnb*-intact controls (Fig. 5A, P15). These findings are consistent with a physiologic role for CTNNB in CGNPs that can be compensated by additional, redundant mechanisms that limit CGNP proliferation.

To determine the role of CTNNB in the *Gsk-3*^{DKO} phenotype, we crossed *Ctnnb*^{cKO} and *Gsk-3*^{DKO} mice to generate the genotype *Math1-Cre/Gsk-3α*$^{-/-}$*/Gsk-3β*$^{loxP/loxP}$*/Ctnnb*$^{loxP/loxP}$ (*Gsk-3/Ctnnb*^{TKO}). We found that *Gsk-3/Ctnnb*^{TKO} mice were markedly less symptomatic than *Gsk-3*^{DKO} mice. While all *Gsk-3*^{DKO} mice failed to survive beyond P22, no *Gsk-3/Ctnnb*^{TKO} mice showed early mortality before the study endpoint of P40 (Fig. 5B). *Gsk-3/Ctnnb*^{TKO} mice were ataxic compared to *Gsk-3*-intact controls, but they were markedly less ataxic, with significantly less frequent falls, compared to littermates with *Gsk-3α/β* co-deletion and intact *Ctnnb* (Fig. 5C).

Consistent with improved motor function, cerebellar growth and organization were largely rescued by co-deletion of *Ctnnb*. In contrast to *Gsk-3*^{DKO} mice, CGNPs in *Gsk-3/Ctnnb*^{TKO} mice at P3 and P7 formed a thick EGL (Fig. 5D). The *Gsk-3/Ctnnb*^{TKO} EGL contained an outer layer of CGNPs expressing p-RB and PCNA, and an inner layer of CDKN1B^{+} CGNPs, as in *Gsk-3*-intact controls (Fig. 5E). Like *Gsk-3*-intact controls, *Gsk-3/Ctnnb*^{TKO} CGNPs did not express CDKN1A (Fig. 5E). Quantitative studies showed that the p-RB^{+} fraction of CGNPs in *Gsk-3/Ctnnb*^{TKO} mice was similar to age-matched controls (Fig. 5F).

Although proliferation was rescued by *Ctnnb* co-deletion, CGNP migration remained profoundly abnormal. Migration defects in *Gsk-3/Ctnnb*^{TKO} cerebella became more apparent over time, as CGNPs failed to move across the Purkinje cell layer to form an IGL and instead formed ectopic collections in the molecular layer (Fig. 5D, adult). To determine if the CGNP migration failure was caused by a lack of radial glial processes, we compared FABP7 immunofluorescence *Gsk-3/Ctnnb*^{TKO} and control mice. In both genotypes, radial glia were identified; however, in the *Gsk-3/Ctnnb*^{TKO} the processes appeared to be less numerous (Fig. 5G). These findings suggest that radial glial, which are present in the *Gsk-3/Ctnnb*^{TKO} mice, may present an anatomic substrate for migration, but also leave open the possibility that CGNP-glial interactions may not function normally. Purkinje neurons, labeled by Calbindin immunofluorescence, were positioned appropriately along the inner margin of the EGL in the *Gsk-3/Ctnnb*^{TKO} mice at P7 (Fig. 5G). However, by P21 this positioning was disrupted, suggesting a non-cell autonomous effect of the CGNP migration failure (Fig. 5D).

Trp53 co-deletion does not rescue the *Gsk-3*^{DKO} phenotype

CDKN1A is known to be induced by p53. To determine if the growth restriction of *Gsk-3*^{DKO} cerebella requires signaling through p53, we tested whether co-deletion of *Trp53* would restore the proliferation of *Gsk-3*^{DKO} CGNPs. We co-deleted *Trp53*, *Gsk-3α* and *Gsk-3β* by crossing mice with a conditional allele of TP53 (*Trp53*$^{loxP/loxP}$) with *Gsk-3*^{DKO} mice to generate the genotype *Math1-Cre/Gsk-3α*$^{-/-}$*/Gsk-3β*$^{loxP/loxP}$*/p53*$^{loxP/loxP}$ (*Gsk-3/p53*^{TKO}). *Gsk-3/p53*^{TKO}

mice developed severe, symptomatic cerebellar hypoplasia similar to the *Gsk-3*^{DKO} phenotype and did not survive beyond P20-22. Like the *Gsk-3*^{DKO}, *Gsk-3/p53*^{TKO} mice did not demonstrate increased apoptotic rates but showed reduced PCNA and p-RB and increased CDKN1B and CDKN1A expression throughout the EGL (Fig. 6A). These studies demonstrate that p53-mediated transcription is not required for the induction of CDKN1A, nor for the premature cell cycle exit and growth failure in *Gsk-3*^{DKO} CGNPs.

Cdkn1a co-deletion fails to rescue proliferation in *Gsk-3*-deleted CGNPs

To determine whether CDKN1A mediates the growth suppressive effect of WNT hyperactivation in *Gsk-3*-deleted cerebella, we bred *Cdkn1a*$^{-/-}$ and *Gsk-3*^{DKO} mouse lines to generate *Math1-Cre/Gsk-3α*$^{-/-}$*/Gsk-3β*$^{loxP/loxP}$*/Cdkn1a*$^{-/-}$ (*Gsk-3/Cdkn1a*^{TKO}) mice. In contrast to *Gsk-3/Ctnnb*^{TKO} animals, *Gsk-3/Cdkn1a*^{TKO} mice showed severe cerebellar hypoplasia (Fig. 6B), with ataxia and early mortality similar to *Gsk-3*^{DKO} mice.

The absence of rescue in *Gsk-3/Cdkn1a*^{TKO} cerebella demonstrates that CDKN1A is not necessary for the CGNP proliferation defect in *Gsk3*-deleted mice. While it remains possible that CDKNA1 induction may be sufficient to stop CGNP proliferation, our data show that additional mechanisms predominantly mediate growth suppression downstream of CTNNB in *Gsk-3*^{DKO} mice. Taken together, these rescue studies show that SHH-driven CGNP proliferation requires GSK-3 to suppress CTNNB-mediated WNT signaling, while CGNP migration requires GSK-3 for a yet uncharacterized mechanism. Consistent with this interpretation, cortical neuron migration is controlled by GSK-3-mediated, WNT-independent processes (Morgan-Smith et al., 2014).

GSK-3 is required for medulloblastoma tumor growth

To determine if *Gsk-3α/β* co-deletion restricted SHH-driven proliferation in medulloblastoma as well as in normal cerebellar development, we examined the effect on *SmoM2*-induced tumorigenesis of deleting *Gsk-3α*, *Gsk-3β*, or both loci. Mice with the genotype *Math1-Cre/SmoM2*$^{loxP/+}$ (*M-Smo*) develop medulloblastoma with 100% frequency by P12 and die by P50 (Schüller et al., 2008; Crowther et al., 2016). We crossed *Math1-Cre*, *Gsk-3*^{DKO} and *SmoM2* mouse lines mice to generate the genotype *Math1-Cre/Gsk-3α*$^{-/-}$*/Gsk-3β*$^{loxP/loxP}$*/SmoM2*$^{loxP/+}$ (*M-Smo/Gsk-3*^{DKO}). Like *Gsk-3*^{DKO} mice, *M-Smo/Gsk-3*^{DKO} animals could not survive beyond weaning at P20-22. The identically short survival of *Gsk-3*^{DKO} mice and *M-Smo/Gsk-3*^{DKO} mice shows that *Gsk-3* deletion consistently limits survival to 3 weeks and precludes using survival time to study the effect of Gsk-3 deletion on medulloblastoma growth in *M-Smo* mice. However, we were able to analyze tumor growth in the pre-weaning period. For this purpose, we compared cerebellar pathology between *M-Smo, M-Smo/Gsk-3*^{DKO}, and littermate controls with the genotypes *Math1-Cre/Gsk-3α*$^{-/-}$*/Gsk-3β*$^{loxP/+}$*/SmoM2*$^{loxP/+}$ (*M-*

Smo/Gsk-3α^{KO}*β*^{HET}) or *Math1-Cre/Gsk-3α*$^{-/+}$*/Gsk-3β*$^{loxP/loxP}$*/SmoM2*$^{loxP/+}$ (*M-Smo/Gsk-3α* ^{HET}*β*^{KO}).

Tumor growth in *M-Smo/Gsk-3*^{DKO} mice was markedly reduced, compared to *M-Smo*, *M-Smo/Gsk-3α* ^{KO}*β*^{HET}*, M-Smo/Gsk-3α* ^{HET}*β*^{KO} genotypes (Fig. 7A,B). PCNA staining at P12 and P15 demonstrated small foci of proliferating cells in the otherwise hypoplastic *M-Smo/Gsk-3*^{DKO} cerebella. Co-staining with CDKN1B also demonstrated pockets of differentiating cells that were absent in the *Gsk-3* intact tumors (Fig. 7C). Immunohistochemistry showed that GSK-3 expression persisted in these small proliferating foci, and was absent in the larger population of non-proliferating cells (Fig. 7D). The overall reduced growth in *Gsk-3*-deleted medulloblastomas, and the close consistently retained GSK-3 in p-RB^{+} tumor cells, together show that GSK-3 is required for SHH-driven proliferation in medulloblastoma.

We investigated whether apoptosis or altered cell cycle regulation played a role in suppressing medulloblastoma growth in *M-Smo/Gsk-3*^{DKO} mice, by staining *M-Smo/Gsk-3*^{DKO} tumors for cC3 and p-RB. We did not detect widespread cC3 expression that would indicate apoptosis (Fig. S3). However, we found significantly increased p-RB expression in *M-Smo/Gsk-3*^{DKO} tumors, compared to *M-Smo/Gsk-3α* ^{KO}*β*^{HET} or *M-Smo/Gsk-3α* ^{HET}*β*^{KO} controls (Fig. 7D,E). These data indicate that *Gsk-3* deletion blocked tumor growth by restricting cell cycle progression, rather than by increasing cell death. We also noted induction of CDKN1A in *M-Smo/Gsk-3*^{DKO} tumors, indicating that the GSK-3/CTNNB/CDKN1A axis that we noted in CGNPs remains intact in SHH-driven medulloblastoma.

GSK-3 inhibition is sufficient to arrest medulloblastoma tumor growth

The growth restriction imposed in tumors by *Gsk-3* deletion suggested that pharmacological GSK-3 inhibition might exert a similarly growth suppressive effect. To avoid the complexity of *in vivo* pharmacokinetics, we used an *in vitro* culture assay to examine the function of GSK-3 in promoting medulloblastoma growth. Briefly, we harvested primary *M-Smo* tumors from P15 mice, dissociated the tumor cells and plated them in serum-free media. We then cultured the dissociated tumors with or without GSK-3 inhibitor CHIR98. After 24 hours, we collected cells for western blot or flow cytometry.

Incubation of dissociated *M-Smo* tumor cells with CHIR98 decreased p-RB, decreased phosphorylated CTNNB (p-CTNNB), and increased CDKN1A (Fig. 7F,G). We also noted a decrease in the inhibitory phosphorylation of GSK-3β, in an apparent homeostatic response to GSK-3 inhibition. The decrease in p-RB in *M-Smo* tumor cells treated CHIR98 was dose dependent, and correlated with decrease in CCND2 expression (Fig. 7H, I, Fig. S4). These

data show that SHH-driven medulloblastoma cells are sensitive to changes in GSK-3 activity that are within the range of modulation that can be achieved through small molecule inhibitors.

Discussion

Our data show that modulating GSK-3 activity can modulate SHH-driven proliferation in cerebellar development and in medulloblastoma. Conditional deletion of both isoforms of *Gsk-3* inhibited cell cycle progression and promoted cell cycle exit in CGNPs and SHH-driven medulloblastomas in mice. Pharmacologic inhibition of GSK-3 produced similar growth suppression. Our molecular studies identified WNT activation and CDKN1A up-regulation as consequences of *Gsk-3α /β* co-deletion. The persistence of CDKN1A expression and cerebellar hypoplasia in *Gsk-3/p53*^{TKO} mice shows that p53 activity is not required for either *Cdkn1a* up-regulation or for the *Gsk-3*^{DKO} phenotype. Rescue studies with co-deletion *Ctnnb* show that growth suppression and abnormal migration are aspects of the *Gsk-3*^{DKO} phenotype that can be dissociated, as *Ctnnb* co-deletion in *Gsk-3/Ctnnb*^{TKO} mice allowed *Gsk-3*-deleted CGNPs to proliferate but not to migrate normally.

Prior studies have alternatively suggested growth-promoting effects and growth-inhibiting effects of GSK-3, in both CGNPs (Knoepfler and Kenney, 2006; Penas et al., 2015) and in other cell types (Kim et al., 2009). In CGNPs, the negative regulation of MYCN by GSK-3 suggested a growth suppressive effect (Knoepfler and Kenney, 2006), while the destabilization of WEE1 by GSK-3 suggested a role in promoting cell cycle progression (Penas et al., 2015). Our *Gsk-3*^{DKO} studies make clear that GSK-3 is required for proliferation, and our *Gsk-3/Ctnnb*^{TKO} studies show that the regulation of the WNT pathway by GSK-3 is sufficient to mediate this effect.

The growth suppression elicited by WNT activation in CGNPs contrasts with the growth-promoting effects of WNT activation in diverse progenitors in both the CNS (Spittaels et al., 2002; Kim et al., 2009; Morgan-Smith et al., 2014) and the gut (Harada et al., 1999; Giles et al., 2003). This growth suppressive response to WNT signaling in CGNPs may be due to their specific reliance of mitogenic SHH signaling. Diverse interactions between SHH and WNT signaling pathways have been proposed. Inhibitory interactions have been identified in the developing neural tube and in colon cancer cells, in which WNT signaling induces GLI3, which inhibits SHH-dependent transcription (Alvarez-Medina et al., 2008; Song et al., 2015). In contrast, activating interactions have also been described epidermal cells, where WNT activation induces GLI1, which activates SHH-dependent transcription (Wang et al., 2018). Our finding that WNT signaling interferes with SHH-driven proliferation is consistent with an antagonistic interaction between these pathways.

Our findings build on previous studies in which constitutive WNT signaling, induced by either a mutant allele of *Ctnnb*, or conditional deletion of *Apc*, impaired cerebellar and medulloblastoma growth (Lorenz et al., 2011; Pöschl et al., 2013). By activating WNT signaling through a loss of function mutation, rather than engineering a gain of function, the deletions of *Apc* (Lorenz et al., 2011) and *Gsk-3* demonstrate a physiologic role for WNT in the normal cerebellum . The hyperproliferation that we found in CGNPs with isolated deletion of *Ctnnb* further support the idea that GSK-3/WNT signaling is part of the normal regulation of cerebellar development. Importantly, GSK-3 is a kinase that is susceptible to specific small molecule inhibitors. Our data suggest a potential deleterious impact of exposure to GSK-3 inhibitors during the period of cerebellar development, as well as the potential for GSK-3 inhibitors to advance the treatment of SHH-driven tumors.

It is important to note that our data support the potential of GSK-3 inhibition specifically in the SHH-driven subset of medulloblastoma. If GSK-3 activity shows the same bivalence in medulloblastoma that is seen in development, other medulloblastoma subtypes may be promoted, rather than suppressed by GSK-3 inhibition. The potential effects of GSK-3 inhibition in Group 3 and Group 4 medulloblastomas are unknown and GSK-3 inhibition in WNT subgroup tumors might be expected to increase proliferation. Within the SHH subgroup however, WNT activation through GSK-3 inhibition may provide a new, targeted approach to therapy.

Materials and Methods

Mouse models

Gsk-3α$^{-/-}$ and *Gsk-3β*$^{loxP/loxP}$ mice were generously shared by Dr. William Snider. *Gsk-3α*$^{-/-}$ harboring an exon 2 deletion and *Gsk-3β*$^{loxP/loxP}$ mice with exon 2 flanked by loxP sites have been previously described (MacAulay et al., 2007; Patel et al., 2008). *Gsk-3α*$^{-/-}$ and *Gsk-3β*$^{loxP/loxP}$ mice were bred with the *Math1-Cre* mouse line (Matei et al., 2005), generously shared by Dr. David Rowitch and Dr. Robert Wechsler-Reya, to produce *Gsk-3*^{DKO} mice (*Math1-Cre/Gsk-3α*$^{-/-}$*/Gsk-3β*$^{loxP/loxP}$).

Conditional *Ctnnb* (*Ctnnb*$^{loxP/loxP}$) knockout mice were generously shared by Dr. Eva Anton. These mice harbor loxP sites flanking exons 2 – 6 of *Ctnnb* as previously described (Brault et al., 2001). *Ctnnb*$^{loxP/loxP}$ were bred with *Math1-Cre* mice to produce *Math1-Cre/Ctnnb*$^{loxP/loxP}$ *(Ctnnb*^{cKO}*)* mice. Alternatively, *Ctnnb*$^{loxP/loxP}$ mice were bred with *Math1-Cre/Gsk-3α*$^{+/-}$*/Gsk-3β*$^{loxP/loxP}$ to generate *Math1-Cre/Gsk-3α*$^{-/-}$*/Gsk-3β*$^{loxP/loxP}$*/Ctnnb*$^{loxP/loxP}$ (*Gsk-3/Ctnnb*^{TKO}). *Tp53*$^{loxP/loxP}$ mice were purchased from the Jackson Laboratory (Marino et al., 2000) and crossed with *Math1-Cre/Gsk-3α*$^{+/-}$*/Gsk-3β*$^{loxP/loxP}$ mice to generate *Math1-Cre/Gsk-*

3α$^{+/-}$*/Gsk-3β*$^{loxP/loxP}$*/tp53*$^{loxP/loxP}$ (*Gsk-3/p53*^{TKO}) mice. *Cdkn1a*$^{-/-}$ mice were purchased from Jackson Laboratories (Deng et al., 1995). These mice were bred with *Math1-Cre/Gsk-3α*$^{+/-}$*/Gsk-3β*$^{loxP/loxP}$ to generate *Math1-Cre/Gsk-3α*$^{-/-}$*/Gsk-3β*$^{loxP/loxP}$*/Cdkn1a*$^{-/-}$ (*Gsk-3/Cdkn1a*^{TKO}) progeny. Littermates heterozygous for *Gsk-3* or *Cdkn1a* were used as controls.

Math1-Cre/Gsk-3α$^{+/-}$*/Gsk-3β*$^{loxP/loxP}$ were crossed with *SmoM2*$^{loxP/loxP}$ mice purchased from Jackson Laboratories (Mao et al., 2006) to produce *Math1-Cre/Gsk-3α*$^{+/-}$*/Gsk-3β*$^{loxP/loxP}$*/SmoM2*$^{loxP/wt}$ (*M-Smo/Gsk-3α*^{HET}*/Gsk-3β*^{KO}), *Math1-Cre/Gsk-3α*$^{-/-}$*/Gsk-3β*$^{loxP/wt}$*/SmoM2*$^{loxP/wt}$ (*M-Smo/Gsk-3α*^{KO}*/Gsk-3β*^{HET}), and *Math1-Cre/Gsk-3α*$^{-/-}$*/Gsk-3β*$^{loxP/loxP}$*/SmoM2*$^{loxP/wt}$ (*M-Smo/Gsk-3*^{DKO}) mice. *SmoM2*$^{loxP/loxP}$ mice were also crossed with *Math1-Cre* mice to produce *Math1-Cre/SmoM2* (M-Smo) progeny.

All mice were genotyped by PCR using primers listed in Table S2. All animal experiments were carried out in accordance with established NIH practices and approved under University of North Carolina Institutional Animal Care and Use Committee Protocols #13-121.0, 15-306.0, 16-099.0, and 18-199. All mice for these experiments were of the species *Mus musculus*, maintained on the C57/BLK6 background.

Cell culture

CGNPs were isolated by size selection and explanted as previously described (Kenney et al., 2003; Lang et al., 2016). Briefly, cerebella were dissected from P5 pups, dissociated with papain using the Papain Dissociation System (#LK003150, Worthington Biochemical Corporation) and selected on a density gradient of ovomucoid inhibitor, then allowed to adhere to coated culture wells in DMEM/F12 (#11320, Life Technologies) with 25 mmol/L KCl, supplemented with heat inactivated FBS (HI-FBS) and N2. After 4 hours, media was replaced with identical serum-free media. Cells were maintained in 0.5 mg/mL SHH (#464SH, R&D Systems) or vehicle (0.1% BSA in 1x PBS).

Where indicated, the specified dose of GSK-3 inhibitor (CHIR-980914, #S2745/ LY2090314, #S7063, Selleckchem) was added to cultures after the first 4 hours and cells were harvested 24 hours after drug treatment. *In vitro* proliferation was assessed by EdU incorporation after a 1 hour exposure to 20 µmol/L EdU. EdU was visualized using the Click-iT™ EdU Alexa Fluor Imaging Kits (#C10337, ThermoFisher Scientific) according to manufacturer's protocol. Cell counts were performed using Olympus CellSens software. Tumor cultures from medulloblastomas freshly harvested from Math1-*Cre/SmoM2* mice were prepared according to the CGNP culture protocol above, with SHH supplementation omitted.

Immunostaining cerebellar sections and quantification

Mouse brains were processed and immunostained as previously described (Crowther et al., 2016; Lang et al., 2016) using antibodies listed in Table S2. EdU was visualized using the Click-iT TM EdU Alexa Fluor Imaging Kits (ThermoFisher Scientific, #C10337) according to manufacturer's protocol. Immunostained sections were counterstained with 200 ng/mL 4'6-diami-dino-2-phenylindole (DAPI/ #D1306, Thermo Fisher Scientific) in 1x PBS for 20 minutes. Stained slides were digitally acquired using an Aperio ScanScope XT (Aperio).

To quantify proliferating cell nuclear antigen (PCNA), CDKN1B/p27, phosphorylated Retinoblastoma (p-RB), CDKN1A, cleaved Caspase-3, BrdU or EdU-positive cells, the EGL region was manually annotated on each section, which was then subjected to automated cell counting using Tissue Studio (Definiens) for fluorescent slides. Quantification of cultured cells was performed by randomly imaging 3 sections of each well and performing cell counts with binary images using the particle analyzer in ImageJ/Fiji. *P*-values were determined by two-tailed Student's *t*-tests where indicated. Adjusted *p*-values for multiple comparisons were determined by ANOVA with Tukey HSD post-hoc testing where indicated.

Cell cycle exit analysis

5-bromo-2-deoxyuridine (BrdU) and 5-ethnynyl-2'-deoxyuridine (EdU) experiments, mice were subjected to intraperitoneal (IP) injection of BrdU (#B23151, ThermoFisher Scientific;100 mg/kg in 25 µl of HBSS). After 24 hours, mice were IP injected with EdU (#A10044, Life Technologies; 40 mg/kg in 25 µl of HBSS) and dissected 2 hours later. Brains were fixed in 4% paraformaldehyde in 1X PBS for 48 hours at 4^{o}C before being processed for histology.

Microarray analysis

RNA was purified from whole P1 cerebella according to manufacturer's protocol (RNeasy Mini Kit, #74104, QIAGEN). RNA quality and quantity were assessed by spectrophotometry, capillary gel electrophoresis, and NanoDrop. Samples were prepared using the Ambion® WT Expression Kit for High-Throughput Robotics (#4440537) and the Affymetrix® HT WT Terminal Labeling and Controls Kit (#901647). We quantified transcripts using the Affymetrix Mouse Gene 2.1 ST 24-Arrays (#902140, Affymetrix) and scanned with the Affymetrix GeneChip Scanner 3000 7G Plus. Data were processed using the Partek Genomics Suite 6.6 standard workflow for expression analysis. Differential gene expression analysis was performed by 2-way ANOVA using Partek or with Signifcance Analysis of Microarrays (SAM) and Gene Set Analysis (GSA) with RStudio Version 1.1.456.

Pathway analysis

Gene sets collected from microarray analysis were subjected to Gene Set Enrichment Analysis (GSEA) using freely available software from the Broad Institute (Mootha et al., 2003; Subramaniana et al., 2005). The Molecular Signatures Database (MSigDB) were used to provide annotated gene sets for comparative analysis and p-values were estimated by 1000 permutations.

Western blot analysis

Cultured cells and whole cerebella were lysed by homogenization in RIPA buffer containing protease inhibitor cocktail, sodium fluoride (NaF), and sodium orthovanadate (Na_3VO_4). Protein concentrations were quantified using the bicinchoninic acid (BCA) method (#23229, Thermo Fisher Scientific) and equal concentrations of protein were resolved on SDS-polyacrylamide gels followed by transfer onto polyvinylidene difluoride membranes. Immunologic analysis was performed on the SNAP i.d. 2.0 Protein Detection System (Millipore) as per manufacturer's protocol with antibodies listed in Table S2. Western blots were developed using the enhanced chemiluminescent SuperSignal West Femto Maximum Sensitivity Substrate (#34095, Thermo Fisher Scientific) and digitized using the C-DiGit blot scanner (LI-COR Biosciences). Quantification was performed using Image Studio Lite software (LI-COR Biosciences).

Flow cytometry analysis

Tumors from *M-Smo/Gsk-3*^{DKO} mice and control, tumor-bearing littermates were harvested and dissociated as described for cell culture studies. Dissociated cells were resuspended in HBSS supplemented with 6g/L glucose and fixed with the Fix & Perm Cell Fixation & Cell Permeabilization Kit (ThermoFisher Scientific). Cells were then stained for FxCycle Violet and p-RB using the antibodies listed in Table S2. Samples were run on the Becton Dickinson LSR Fortressa and data was analyzed with FlowJo V10.

Acknowledgements

We thank the UNC Center for Gastrointestinal Biology and Disease Histology Core for processing tissue sections and staining for H&E, (P30 DK 03987), Gabriela De la Cruz and Stephanie Cohen in the UNC Translational Pathology Laboratory (TPL) for help staining, digitizing, and quantifying sections. TPL is supported, in part, by grants from the NCI (5P30CA016086-42), NIH (U54-CA156733), NIEHS (5 P30 ES010126-17), UCRF, and NCBT (2015-IDG-1007). We also thank the UNC Flow Cytometry Core Facility for assistance with FACS. We are thankful to Jeremy Simon (UNC Neuroscience Bioinformatics Core) for his assistance with microarray analysis, who is supported by The Eunice Kennedy Shriver National Institute of Child Health and Human Development (U54HD079124) and NINDS (P30NS045892). We thank David Rowitch (UCSF, San Francisco, CA) and Robert Wechsler-Reya (Sanford-Burnham Medical Research Institute, La Jolla, CA) for the *Math1-Cre* mice, Dr. William D. Snider (UNC Neuroscience Center) for the *Gsk-3α*$^{-/-}$*/Gsk-3β*$^{loxP/loxP}$ mice, and Dr. Eva Anton (UNC Neuroscience Center) for the *Ctnnb*^{cKO} mice.

Funding

J.K.O. is supported by an F31 award from the NINDS (1F31NS100489). T.R.G. is supported by grants from the NINDS (R01NS088219, R01NS102627, R01NS106227) and the St. Baldrick's Foundation.

Competing interests

The authors declare no competing or financial interests.

Data availability

Microarray data are available at Gene Expression Omnibus (GSE135463).

References

Akiyoshi, T., Nakamura, M., Koga, K., Nakashima, H., Yao, T., Tsuneyoshi, M., Tanaka, M. and Katano, M. (2006). Gli1, downregulated in colorectal cancers, inhibits proliferation of colon cancer cells involving Wnt signalling activation. *Gut* **55**, 991–999.

Alvarez-Medina, R., Cayuso, J., Okubo, T., Takada, S. and Marti, E. (2008). Wnt canonical pathway restricts graded Shh/Gli patterning activity through the regulation of Gli3 expression. *Development* **135**, 237–247.

Bengoa-Vergniory, N. and Kypta, R. M. (2015). Canonical and noncanonical Wnt signaling in neural stem/progenitor cells. *Cell. Mol. Life Sci.*

Brault, V., Moore, R., Kutsch, S., Ishibashi, M., Rowitch, D. H., Mcmahon, A. P., Sommer, L., Boussadia, O. and Kemler, R. (2001). Inactivation of the β -catenin gene by Wnt1-Cre-mediated deletion results in dramatic brain malformation and failure of craniofacial development. **1264**, 1253–1264.

Chizhikov, V. and Millen, K. J. (2003). Development and malformations of the cerebellum in mice. *Mol. Genet. Metab.* **80**, 54–65.

Cole, A. R. (2012). GSK3 as a Sensor Determining Cell Fate in the Brain. *Front. Mol. Neurosci.* **5**, 1–10.

Crowther, A. J., Ocasio, J. K., Fang, F., Meidinger, J., Wu, J., Deal, A. M., Chang, S. X., Yuan, H., Schmid, R., Davis, I., et al. (2016). Radiation Sensitivity in a Preclinical Mouse Model of Medulloblastoma Relies on the Function of the Intrinsic Apoptotic Pathway. *Cancer Res.* **76**, 3211–3223.

Deng, C., Zhang, P., Harper, J. W., Elledge, S. J. and Leder, P. (1995). Mice lacking p21CIP1/WAF1 undergo normal development, but are defective in G1 checkpoint control. *Cell* **82**, 675–684.

Garel, C., Fallet-Bianco, C. and Guibaud, L. (2011). The fetal cerebellum: development and common malformations. *J. Child Neurol.* **26**, 1483–92.

Gibson, P., Tong, Y., Robinson, G., Thompson, M. C., Currle, D. S., Eden, C., Kranenburg, T. A., Hogg, T., Poppleton, H., Martin, J., et al. (2010). Subtypes of medulloblastoma have distinct developmental origins. *Nature* **468**, 1095–1099.

Giles, R. H., Van Es, J. H. and Clevers, H. (2003). Caught up in a Wnt storm: Wnt signaling in cancer. *Biochim. Biophys. Acta - Rev. Cancer* **1653**, 1–24.

Grimmer, M. R. and Weiss, W. A. (2006). Childhood tumors of the nervous system as disorders of normal development. *Curr. Opin. Pediatr.* **18**, 634–638.

Hagen, T. and Vidal-Puig, A. (2002). Characterisation of the phosphorylation of beta-catenin at the GSK-3 priming site Ser45. *Biochem. Biophys. Res. Commun.* **294**, 324–8.

Harada, N., Tamai, Y., Ishikawa, T. O., Sauer, B., Takaku, K., Oshima, M. and Taketo, M. M. (1999). Intestinal polyposis in mice with a dominant stable mutation of the β-catenin gene. *EMBO J.* **18**, 5931–5942.

Jho, E., Zhang, T., Domon, C., Joo, C.-K., Freund, J.-N. and Costantini, F. (2002). Wnt/β-catenin/Tcf signaling induces the transcription of Axin2, a negative regulator of the signaling pathway. *Mol. Cell. Biol.* **22**, 1172–83.

Kenney, A. M. and Rowitch, D. H. (2002). Sonic hedgehog Promotes G1 Cyclin Expression and Sustained Cell Cycle Progression in Mammalian Neuronal Precursors. *Mol. Cell. Biol.* **20**, 9055–9067.

Kenney, A. M., Cole, M. D. and Rowitch, D. H. (2003). Nmyc upregulation by sonic hedgehog signaling promotes proliferation in developing cerebellar granule neuron precursors. *Development* **130**, 15–28.

Kim, W.-Y., Wang, X., Wu, Y., Doble, B. W., Patel, S., Woodgett, J. R. and Snider, W. D. (2009). GSK-3 is a master regulator of neural progenitor homeostasis. *Nat. Neurosci.* **12**, 1390–1397.

Knoepfler, P. S. and Kenney, A. M. (2006). Neural precursor cycling at sonic speed: N-Myc pedals, GSK-3 brakes. *Cell Cycle* **5**, 47–52.

Lang, P. Y. and Gershon, T. R. (2018). A New Way to Treat Brain Tumors: Targeting Proteins Coded by Microcephaly Genes? *BioEssays* **40**, 1–14.

Lang, P. Y., Nanjangud, G. J., Sokolsky-Papkov, M., Shaw, C., Hwang, D., Parker, J. S., Kabanov, A. V. and Gershon, T. R. (2016). ATR maintains chromosomal integrity during postnatal cerebellar neurogenesis and is required for medulloblastoma formation. *Development* **143**, 4038–4052.

Li, X.-J., Zhang, X., Johnson, M. A., Wang, Z.-B., Lavaute, T. and Zhang, S.-C. (2009). Coordination of sonic hedgehog and Wnt signaling determines ventral and dorsal telencephalic neuron types from human embryonic stem cells. *Development* **136**, 4055–4063.

Lorenz, A., Deutschmann, M., Ahlfeld, J., Prix, C., Koch, A., Smits, R., Fodde, R., Kretzschmar, H. A. and Schuller, U. (2011). Severe Alterations of Cerebellar Cortical Development after Constitutive Activation of Wnt Signaling in Granule Neuron Precursors. *Mol. Cell. Biol.* **31**, 3326–3338.

MacAulay, K., Doble, B. W., Patel, S., Hansotia, T., Sinclair, E. M., Drucker, D. J., Nagy, A. and Woodgett, J. R. (2007). Glycogen Synthase Kinase 3α-Specific Regulation of Murine Hepatic Glycogen Metabolism. *Cell Metab.* **6**, 329–337.

Machold, R. and Fishell, G. (2005). Math1 Is Expressed in Temporally Discrete Pools of Cerebellar Rhombic-Lip Neural Progenitors. *Neuron* **48**, 17–24.

Mao, J., Ligon, K. L., Rakhlin, E. Y., Thayer, S. P., Bronson, R. T., Rowitch, D. and McMahon, A. P. (2006). A novel somatic mouse model to survey tumorigenic potential applied to the Hedgehog pathway. *Cancer Res.* **66**, 10171–10178.

Marino, S., Vooijs, M., Van Der Gulden, H., Jonkers, J. and Berns, A. (2000). Induction of medulloblastomas in p53-null mutant mice by somatic inactivation of Rb in the external granular layer cells of the cerebellum. *Genes Dev.* **14**, 994–1004.

Marzban, H., Del Bigio, M. R., Alizadeh, J., Ghavami, S., Zachariah, R. M. and Rastegar, M. (2015). Cellular commitment in the developing cerebellum. *Front. Cell. Neurosci.* **8**, 1–26.

Matei, V., Pauley, S., Kaing, S., Rowitch, D., Beisel, K. W., Morris, K., Feng, F., Jones, K., Lee, J. and Fritzsch, B. (2005). Smaller inner ear sensory epithelia in Neurog1 null mice are related to earlier hair cell cycle exit. *Dev. Dyn.* **234**, 633–650.

Mootha, V. K., Lindgren, C. M., Eriksson, K., Subramanian, A., Sihag, S., Lehar, J., Puigserver, P., Carlsson, E., Ridderstråle, M., Laurila, E., et al. (2003). PGC-1α-responsive genes involved in oxidative phosphorylation are coordinately downregulated in human diabetes. *Nat. Genet.* **34**, 267–273.

Morgan-Smith, M., Wu, Y., Zhu, X., Pringle, J. and Snider, W. D. (2014). GSK-3 signaling in developing cortical neurons is essential for radial migration and dendritic orientation. *Elife* **3**, 1–24.

Northcott, P. A., Korshunov, A., Pfister, S. M. and Taylor, M. D. (2012). The clinical implications of medulloblastoma subgroups. *Nat. Rev. Neurol.* **8**, 340–351.

Patel, S., Doble, B. W., MacAulay, K., Sinclair, E. M., Drucker, D. J. and Woodgett, J. R. (2008). Tissue-Specific Role of Glycogen Synthase Kinase 3 in Glucose Homeostasis and Insulin Action. *Mol. Cell. Biol.* **28**, 6314–6328.

Penas, C., Mishra, J. K., Wood, S. D., Schürer, S. C., Roush, W. R. and Ayad, N. G. (2015). GSK3 inhibitors stabilize Wee1 and reduce cerebellar granule cell progenitor proliferation. *Cell Cycle* **14**, 417–424.

Polkinghorn, W. R. and Tarbell, N. J. (2007). Medulloblastoma: tumorigenesis, current clinical paradigm, and efforts to improve risk stratification. *Nat. Clin. Pract. Oncol.* **4**, 295–304.

Pöschl, J., Grammel, D., Dorostkar, M. M., Kretzschmar, H. A. and Schüller, U. (2013). Constitutive activation of β-Catenin in neural progenitors results in disrupted proliferation and migration of neurons within the central nervous system. *Dev. Biol.* **374**, 319–332.

Pöschl, J., Bartels, M., Ohli, J., Bianchi, E., Kuteykin-Teplyakov, K., Grammel, D., Ahlfeld, J. and Schüller, U. (2014). Wnt/β-catenin signaling inhibits the Shh pathway and impairs tumor growth in Shh-dependent medulloblastoma. *Acta Neuropathol.* **127**, 605–7.

Roussel, M. F. and Hatten, M. E. (2011). Cerebellum: Development and medulloblastoma. In *Current topics in developmental biology*, pp. 235–282. Elsevier Inc.

Sato, N., Meijer, L., Skaltsounis, L., Greengard, P. and Brivanlou, A. H. (2004). Maintenance of pluripotency in human and mouse embryonic stem cells through activation of Wnt signaling by a pharmacological GSK-3-specific inhibitor. *Nat. Med.* **10**, 55–63.

Schuller, U. and Rowitch, D. H. (2007). B-Catenin Function Is Required for Cerebellar Morphogenesis. *Brain Res.* **1140**, 161–169.

Schüller, U., Heine, V. M., Mao, J., Kho, A. T., Dillon, A. K., Han, Y.-G., Huillard, E., Sun, T., Ligon, A. H., Qian, Y., et al. (2008). Acquisition of Granule Neuron Precursor Identity Is a Critical Determinant of Progenitor Cell Competence to Form Shh-Induced Medulloblastoma. *Cancer Cell* **14**, 123–134.

Song, L., Li, Z. Y., Liu, W. P. and Zhao, M. R. (2015). Crosstalk between Wnt/β-catenin and Hedgehog/Gli signaling pathways in colon cancer and implications for therapy. *Cancer Biol. Ther.* **16**, 1–7.

Spittaels, K., Haute, C. V. A. N. D. E. N., Dorpe, J. V. A. N., Terwel, D., Vandezande, K., Lasrado, R., Bruynseels, K., Irizarry, M., Verhoye, M., Lint, J. V. A. N., et al. (2002). Neonatal neuronal overexpression of glycogen synthase kinase-3 beta reduces brain size in transgenic mice. **113**, 797–808.

Subramaniana, A., Tamayo, P., Mootha, V. K., Mukherjee, S., Ebert, B. L., Gillettea, M. A., Paulovich, A., Pomeroy, S. L., Goluba, T. R., Lander, E. S., et al. (2005). Gene set enrichment analysis: A knowledge-based approach for interpreting genome-wide expression profiles. *Proc. Natl. Acad. Sci. U. S. A.* **102**, 15545–15550.

Ten Donkelaar, H. J. and Lammens, M. (2009). Development of the human cerebellum

and its disorders. *Clin. Perinatol.* **36**, 513–30.

Ulloa, F. and Martí, E. (2010). Wnt won the war: Antagonistic role of Wnt over Shh controls dorso-ventral patterning of the vertebrate neural tube. *Dev. Dyn.* **239**, 69–76.

Vladoiu, M. C., El-hamamy, I., Donovan, L. K., Farooq, H., Holgado, B. L., Sundaravadanam, Y., Ramaswamy, V., Hendrikse, L. D., Kumar, S., Mack, S. C., et al. (2019). Childhood cerebellar tumours mirror conserved fetal transcriptional programs. *Nature*.

Wang, V. Y., Rose, M. F. and Zoghbi, H. Y. (2005). Math1 expression redefines the rhombic lip derivatives and reveals novel lineages within the brainstem and cerebellum. *Neuron* **48**, 31–43.

Wang, Y., Lin, P., Wang, Q., Zheng, M. and Pang, L. (2018). Wnt3a-regulated TCF4/β-catenin complex directly activates the key hedgehog signalling genes Smo and Gli1. *Exp. Ther. Med.* **16**, 2101–2107.

Wechsler-Reya, R. J. and Scott, M. P. (1999). Control of neuronal precursor proliferation in the cerebellum by Sonic Hedgehog. *Neuron* **22**, 103–14.

Yang, Z., Ellis, T., Markant, S. L., Read, T., Jessica, D., Bourboulas, M., Schüller, U., Machold, R., Fishell, G., David, H., et al. (2009). Medulloblastoma can be Initiated by Deletion of patched in Lineage-Restricted Progenitors or Stem Cells. **14**, 135–145.

Yeste-Velasco, M., Folch, J., Trullàs, R., Abad, M. A., Enguita, M., Pallàs, M. and Camins, A. (2007). Glycogen synthase kinase-3 is involved in the regulation of the cell cycle in cerebellar granule cells. *Neuropharmacology* **53**, 295–307.

Zechner, D., Fujita, Y., Hülsken, J., Müller, T., Walther, I., Taketo, M. M., Bryan Crenshaw, E., Birchmeier, W. and Birchmeier, C. (2003). β-Catenin signals regulate cell growth and the balance between progenitor cell expansion and differentiation in the nervous system. *Dev. Biol.* **258**, 406–418.

Zhao, Z., Lu, P., Zhang, H., Xu, H., Gao, N., Li, M. and Liu, C. (2014). Nestin positively regulates the Wnt/β-catenin pathway and the proliferation, survival and invasiveness of breast cancer stem cells. *Breast Cancer Res.* **16**, 408.

Zinke, J., Schneider, F. T., Harter, P. N., Thom, S., Ziegler, N., Toftgård, R., Plate, K. H. and Liebner, S. (2015). β-Catenin-Gli1 interaction regulates proliferation and tumor growth in medulloblastoma. *Mol. Cancer* **14**, 17.

Figures

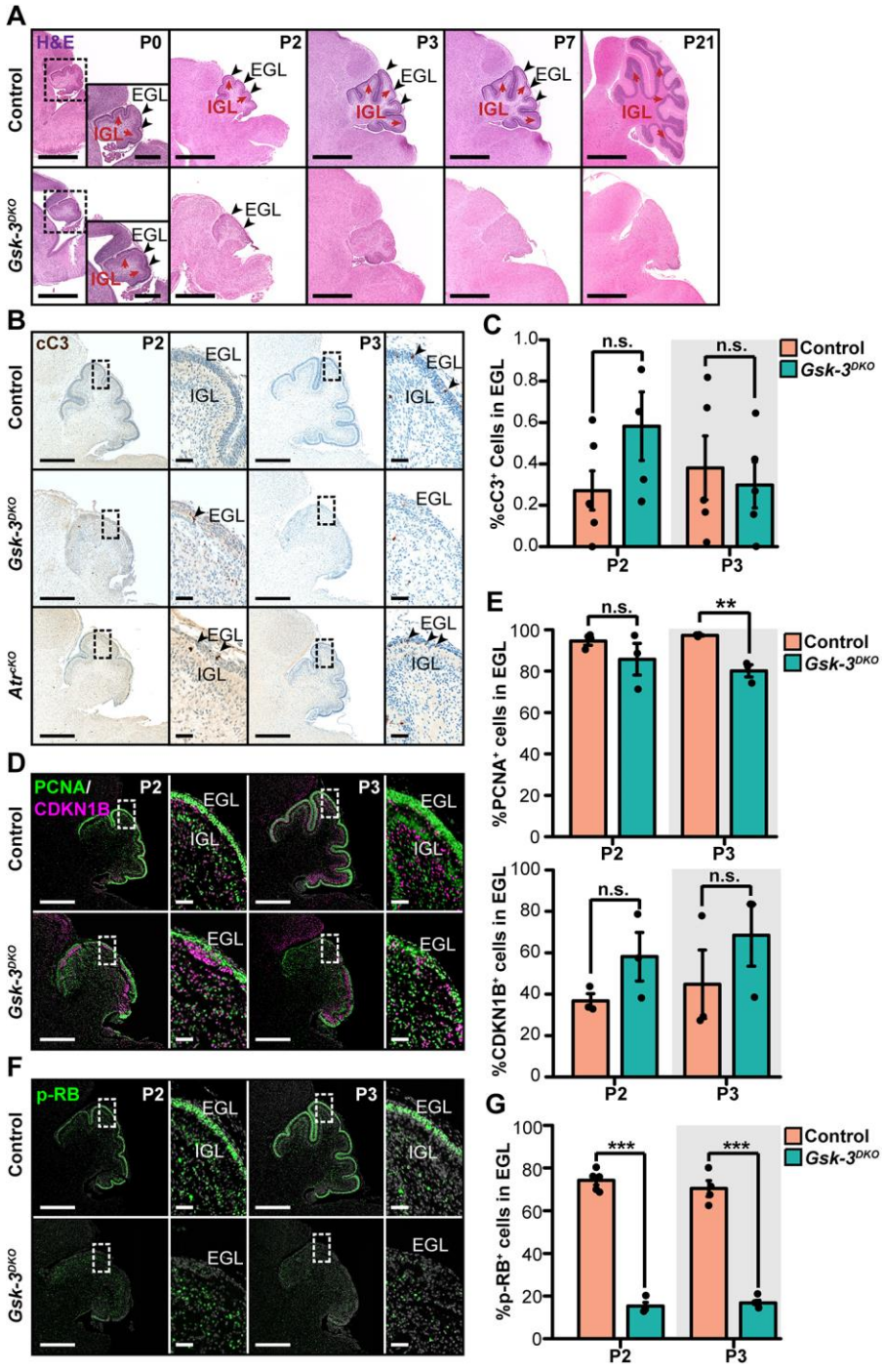

Fig. 1. *Gsk-3* deletion in CGNPs causes cerebellar hypoplasia early in development without inducing apoptosis. (**A**) Representative H&E-stained sagittal cerebellar sections of *Gsk-3*^{DKO} cerebella compared to *Gsk-3* intact littermate controls. Black arrowheads identify the EGL. Red arrows identify the IGL. (**B**) Representative sagittal cerebellar sections of *Gsk-3*^{DKO} mice and *Gsk-3* intact controls stained for cleaved Caspase-3 (cC3). *Atr*^{cKO} cerebella

were used as positive controls for apoptosis. Black arrowheads highlight positive cells. (**C**) Quantification of $cC3^+$ cells in the EGL at P2 and P3 performed using replicates of the genotypes presented in **(B)** (n=6 per genotype at P2; n=5 per genotype at P3). (**D**) Immunostaining for PCNA and CDKN1B in *Gsk-3* deleted and littermate control cerebella at P2 and P3. (**E**) Quantification of the $PCNA^+$ and $CDKN1A^+$ cells in the EGL at P2 or P3 using replicates of the genotypes presented in 1D (n=3 per genotype). (**F**) Immunostaining for phosphorylated RB (p-RB) in $Gsk\text{-}3^{DKO}$ and littermate control cerebella. (**G**) Quantification of the $p\text{-}RB^+$ cells in the EGL using replicates of the genotypes presented in **(F)** (n=3 per genotype). The regions of the higher magnification images are outlined by rectangles on the low magnification images. In (**D,F**), nuclei counterstained with DAPI are pseudocolored gray. Scale bars measure 1 mm for low magnification images and 500 μm for higher magnification images in (**A**), and 500 μm for low magnification images and 50 μm for higher magnification images in (**B**, **D**, **F**). Error bars indicate SEM. Significance for quantification is denoted by *p<0.05, **p<0.01, ***p<0.001 as determined by student's t-test. Dots represent replicate mice.

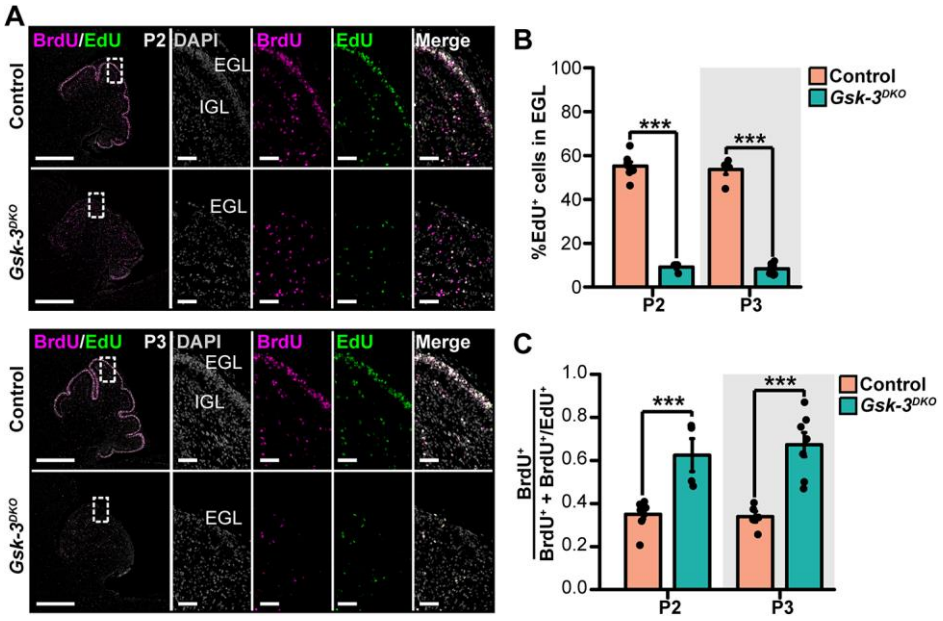

Fig. 2. GSK-3 is required for CGNP proliferation and cell cycle progression. (A) Representative *Gsk-3* intact and *Gsk-3*^{DKO} cerebella pulse-labeled by BrdU and EdU at the indicated age. **(B)** Quantification of EdU^{+} cells in the EGL of *Gsk-3*^{DKO} or littermate control cerebella from replicate mice as in **(A)** (P2 control: n=8; P2 *Gsk-3*^{DKO}: n=4; P3 control: n=5; P3 *Gsk-3*^{DKO}: n=7). **(C)** Quantification of cell cycle exit fraction as determined by the proportion of BrdU cells not co-expressing EdU divided by the total BrdU^{+} population in *Gsk-3*-deleted CGNPs as compared to littermate controls from replicate mice as in **(A)** and **(B)**. Error bars indicate SEM. Dots represent replicate mice. Statistical significance is denoted by *p<0.05, **p<0.01, ***p<0.001 as determined by student's t-test **(B, C)**. In (**A,B**), nuclei counterstained with DAPI are pseudocolored gray. The regions of the higher magnification images are outlined by rectangles on the low magnification images. Scale bars measure 500 μm for low magnification images and 50 μm for higher magnification images.

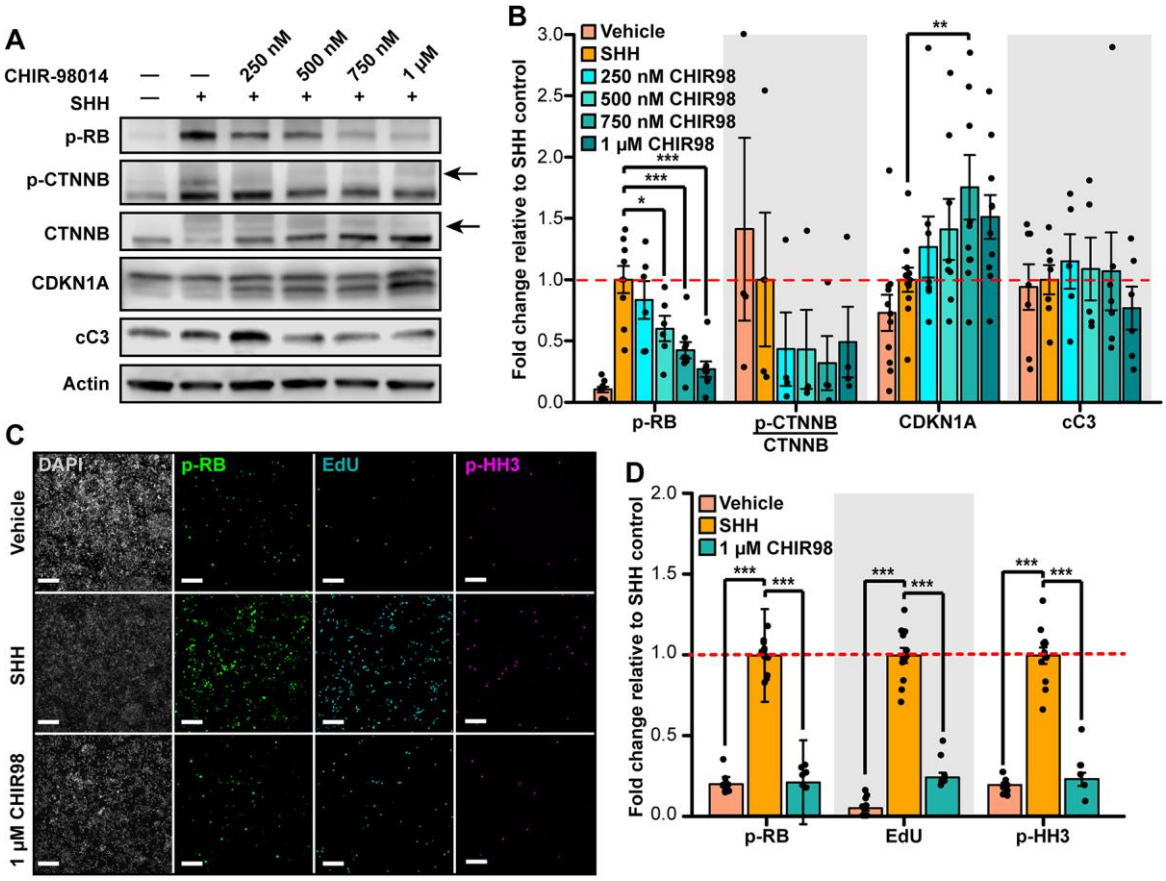

Fig. 3. GSK-3 inhibition blocks proliferation in vitro. (A) Representative western blot images show p-RB, p-CTNNB, and CDKN1A protein levels in response to increasing concentrations of the GSK-3 inhibitor CHIR98. **(B)** Quantification of western blot data as in **(A)**, with luminescence normalized to actin and expressed as fold change relative to SHH control ($n \geq 5$ per condition for p-RB; $n \geq 4$ per condition for p-CTNNB/CTNNB; $n \geq$ at least 7 per condition for CDKN1A; $n \geq 6$ per condition for cC3). Statistical significance denoted by *p<0.05, **p<0.01, ***p<0.001 as determined by ANOVA with Tukey HSD post-hoc test. **(C)** Representative DAPI-stained and immunofluorescence images of cultured CGNPs treated as indicated and pulse-labeled with EdU 1 hour before fixation. Cells were stained for p-RB, EdU, and p-HH3. **(D)** Quantification of p-RB, EdU, and p-HH3 from replicate cultures (n=12 per condition) as in **(C)**, expressed as fold change relative to SHH control. Scale bars measure 50 μm. Error bars indicate SEM. Dots represent replicate mice. Statistical significance denoted by *p<0.05, **p<0.01, ***p<0.001 as determined by student's t-test.

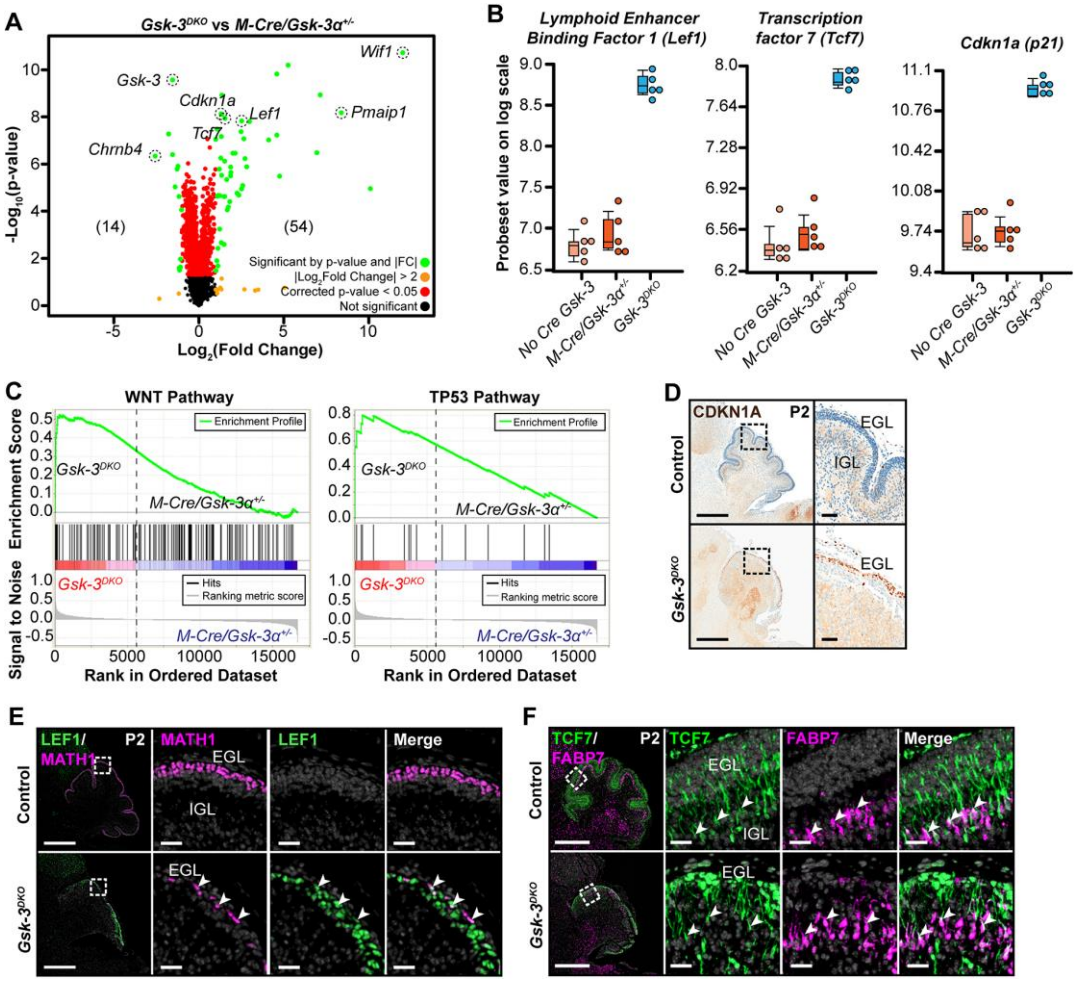

Fig. 4. Transcriptional analysis reveals upregulation of WNT/CDKN1A signaling in *Gsk-3^{DKO}* mice. (A) Volcano plot of $\log_2$(FC) vs. -$\log_{10}$(p-value) with color threshold (green dots) set at |$\log_2$(FC)| > 2 and FDR < 0.05 (lines). Significant genes are labeled and outlined in black dashed circles. Legend indicating dot color-coding in the bottom right corner (n=5 per genotype). **(B)** Dot plots show representative genes that were upregulated in *Gsk-3* mutants, including WNT markers *Lef1* and *Tcf7*, and *Cdkn1a*, as compared to *M-Cre/Gsk-3α$^{+/-}$* and *No-Cre/Gsk-3* controls. **(C)** GSEA analysis demonstrates upregulation of WNT and p53 signaling pathways in *Gsk-3* deleted cerebella as compared to *M-Cre/Gsk-3α$^{+/-}$* controls. **(D)** Immunostaining of select gene markers **(D)** CDKN1A, **(E)** LEF1 and **(F)** TCF7 identified from the microarray in *Gsk-3^{DKO}* mice and littermate controls, co-stained with **(E)** MATH1 or **(F)** FABP7. In (**E,F**), nuclei counterstained with DAPI are pseudocolored gray. The regions of the higher magnification images are outlined by rectangles on the low magnification images. Scale bars measure 500 μm for low magnification images and 25 μm for higher magnification images.

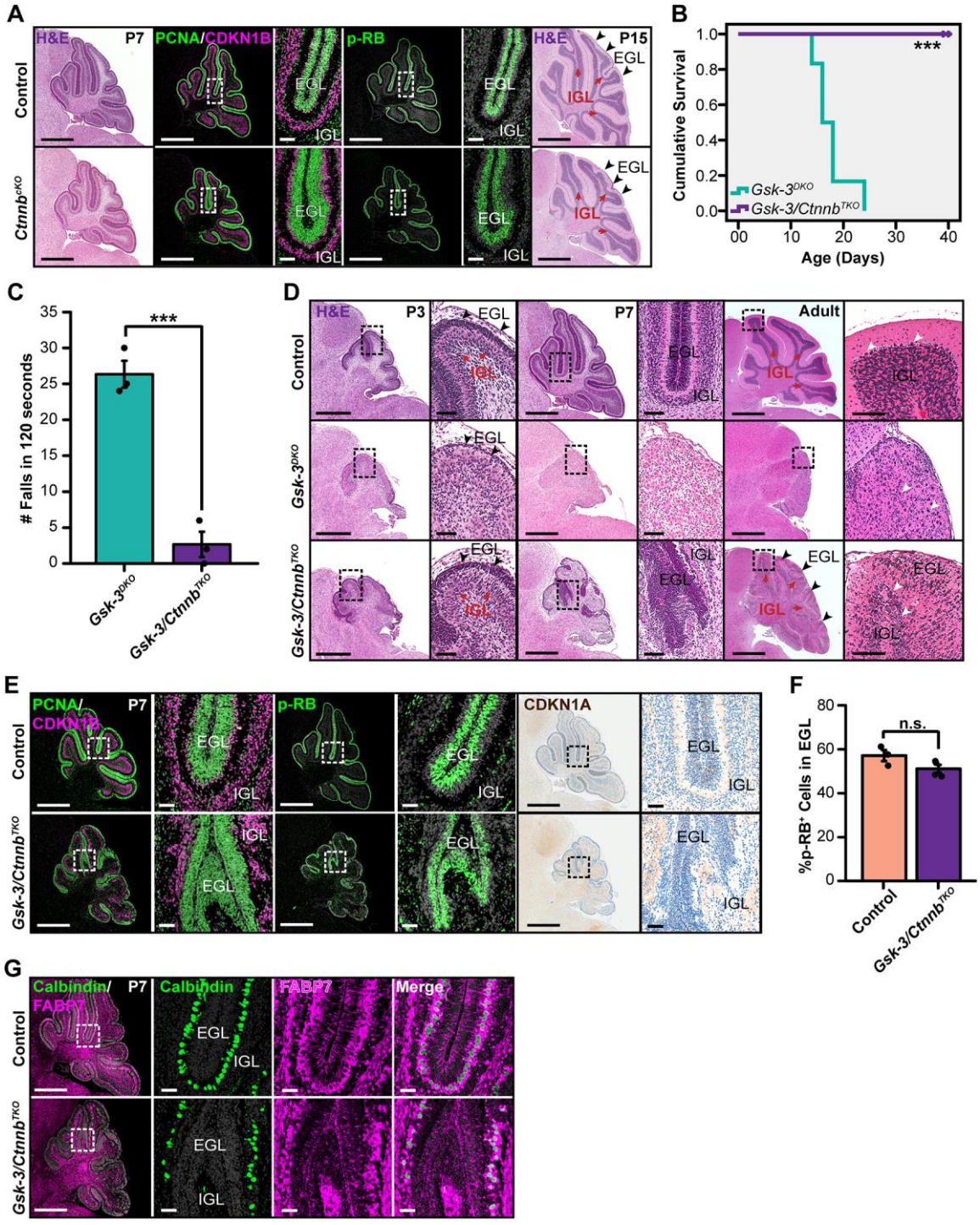

Fig. 5. CTNNB modulates CGNP proliferation downstream of GSK-3. (A) Comparison of *Ctnnb*^{cKO} mice and littermate controls, in representative cerebellar sections stained with H&E at P7 and P15, and for PCNA/CDKN1B and p-RB at P7. **(B)** Survival curve demonstrating cumulative survival of *Gsk-3/Ctnnb*^{TKO} mice as compared to *Gsk-3*^{DKO} mice (n=6 per genotype). Statistical significance is denoted by *p<0.05, **p<0.01, ***p<0.001 as determined by the Kaplan-Meier method and log rank test. **(C)** Comparison of *Gsk-3*^{DKO} and

Gsk-3/Ctnnb^{TKO} mice by number of falls per 120s (n=3 per genotype). **(D)** Comparison of *Gsk-3*^{DKO} and *Gsk-3/Ctnnb*^{TKO} cerebella, in representative H&E stained sections at indicated ages. Black arrowheads highlight the EGL. Red arrowheads highlight the IGL. White arrowheads in right panel highlight examples of Purkinje neurons. **(E)** Representative control and *Gsk-3/Ctnnb*^{TKO} cerebellar sections stained for PCNA/CDKN1B, p-RB, and CDKN1A . **(F)** Quantification of p-RB^{+} cells in the EGL of *Gsk-3/Ctnnb*^{TKO} mice (n=4) and *Gsk-3*-intact littermate controls (n=3), from replicate mice as in **(E)**. **(G)** Comparison of *Gsk-3/Ctnnb*^{TKO} mice and littermate controls in representative Calbindin and FABP7-stained sections. In (**A,E,G**), nuclei counterstained with DAPI are pseudocolored gray. The regions of the higher magnification images are outlined by rectangles on the low magnification images. Scale bars measure 700 μm for low magnification images and 50 μm for higher magnification images in **(A, D,G)**. Error bars indicate SEM. Dots represent replicate mice. Statistical significance is denoted by *p<0.05, **p<0.01, ***p<0.001 as determined by student's t-test.

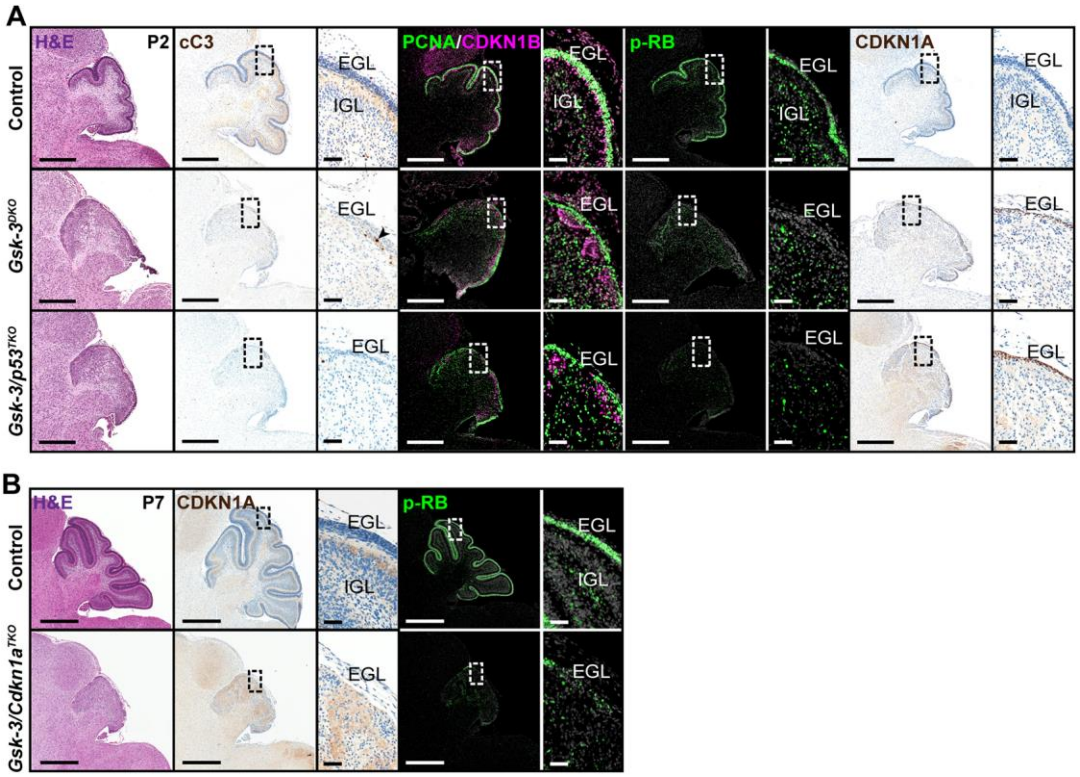

Fig. 6. Reduced proliferation in *Gsk-3*-mutants is independent of p53 and CDKN1A. (A) Comparison of Control, *Gsk-3*^{DKO} and *Gsk-3/p53*^{TKO} cerebella, in representative H&E, PCNA/CDKN1B, p-RB, and CDKN1A stained cerebellar sections **(B)** Comparison of control and *Gsk-3/Cdkn1a*^{TKO} cerebella in representative H&E, CDKN1A, or p-RB-stained sections. In (**A,B**), nuclei counterstained with DAPI are pseudocolored gray. The regions of the higher magnification images are outlined by rectangles on the low magnification images. Scale bars measure 500 μm for low magnification images and 50 μm for higher magnification images in **(A)** or 700 μm for low magnification images and 50 μm for higher magnification images in **(B)**.

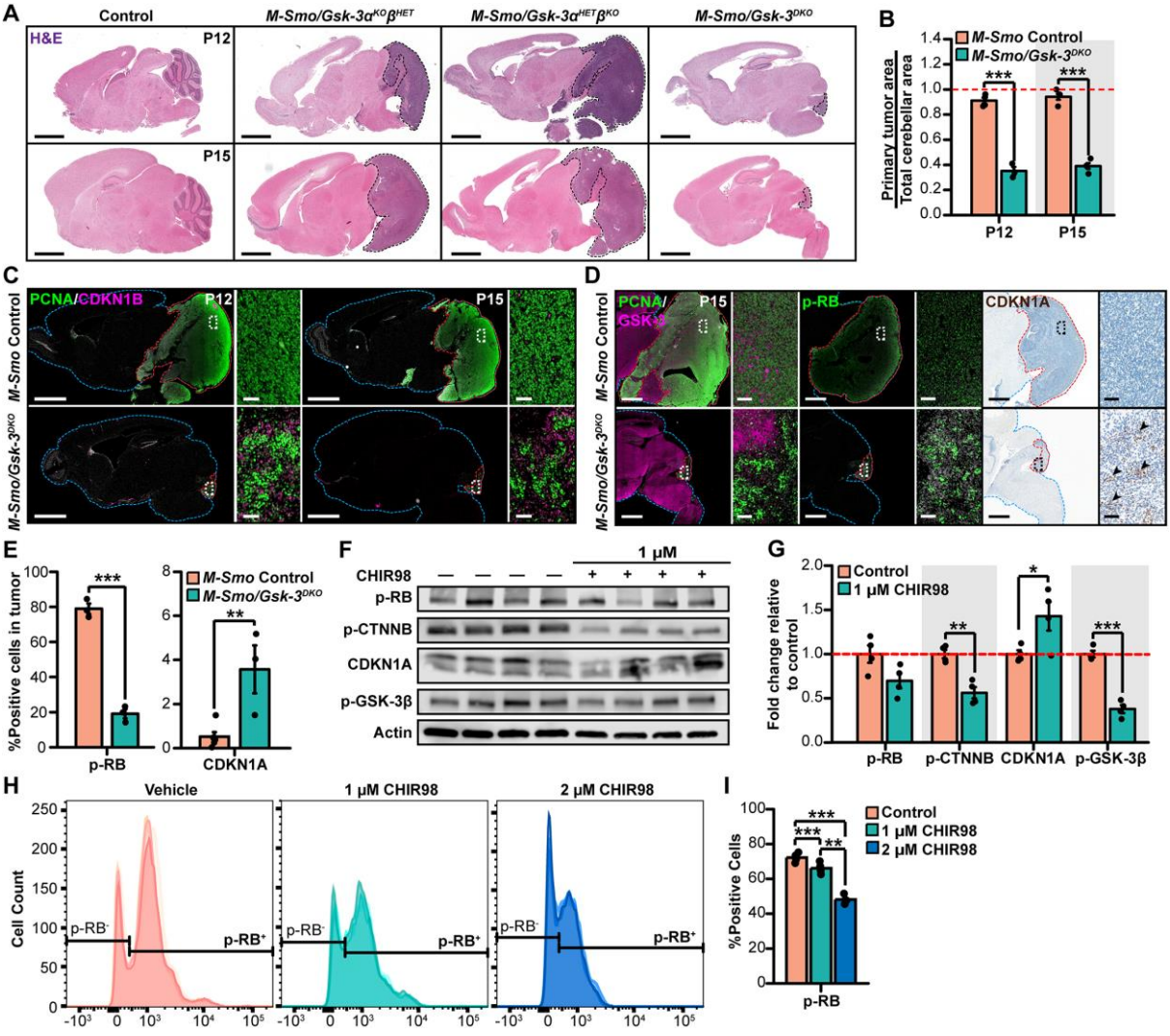

Fig. 7. GSK-3 is required for Shh-driven medulloblastoma tumor growth. (A) Comparison of cerebellar regions in *M-Smo/Gsk-3*^{DKO} mice and *Gsk-3* intact *Smo*-mutant in representative H&E-stained cerebellar sections at P12 and P15. Primary tumor area outlined with a black dashed line. **(B)** Comparison of tumor area in *Gsk-3*-deleted and control tumors, using replicates of the genotypes in **(A)**, normalized to total cerebellar area at P12 and P15 (n=4 for P12 control; n=3 per genotype) **(C)** Comparison of PCNA and CDKN1B immunostaining in *Gsk-3*-deleted and control tumors, using replicates of the genotypes in **(A)**. **(D)** Comparison of PCNA and GSK-3, p-RB, and CDKN1A immunostaining in *Gsk-3*-deleted and control tumors, using replicates of the genotypes in **(A)**. **(E)** Quantification of p-RB^{+} and CDKN1A^{+} cells comparing *Gsk-3*-deleted and control tumors (P12 control: n=4; P12 *Gsk-3*^{DKO}: n=3; P15 control: n=5; P15 *Gsk-3*^{DKO}: n=3). **(F)** Representative western blot images of p-RB, p-CTNNB, CDKN1A, p-GSK-3β, and actin protein levels in cultured *M-Smo* tumor cells treated with or without 1 μM of the GSK-3 inhibitor CHIR-98014. **(G)**

Quantification of western blot data from replicates as in **(F)**, normalized to actin and expressed as fold change relative to control tumor cells (n=4 per condition). **(H)** Histograms of p-RB^{+} and p-RB^{-} tumor cells treated *in vitro* with vehicle, 1 μM, or 2 μM of CHIR98. **(I)** Quantification of p-RB^{+} cells in biological replicates from **(H)** (n=4 per condition). Error bars indicate SEM. Dots represent replicate mice. Significance is denoted by *p<0.05, **p<0.01, ***p<0.001 as determined by student's t-test. In (**C, D**), the edges of the brain are outlined in blue and the edges of the tumor are outlined in red and nuclei, counterstained with DAPI are pseudocolored gray. The regions of the higher magnification images are outlined by rectangles on the low magnification images. Scale bars measure 2 mm for low magnification images and 50 μm for higher magnification images.

Figure S1

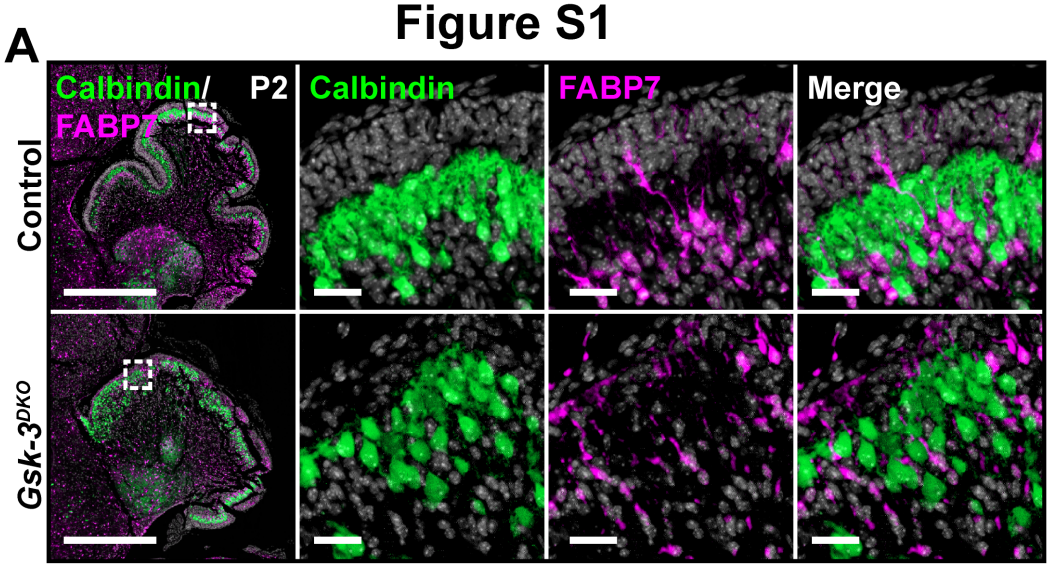

Fig. S1. Bergmann glia and Purkinje neurons extend processes in *Gsk-3^{DKO}* cerebella. (A) Representative sagittal sections of cerebella from control and *Gsk-3^{DKO}* mice at P2 and P3 stained for the Purkinje cell marker, Calbindin, and the Bergmann glial marker, FABP7. Scale bars measure 500 µm and 25 µm in insets. Nuclei counterstained with DAPI are pseudocolored gray.

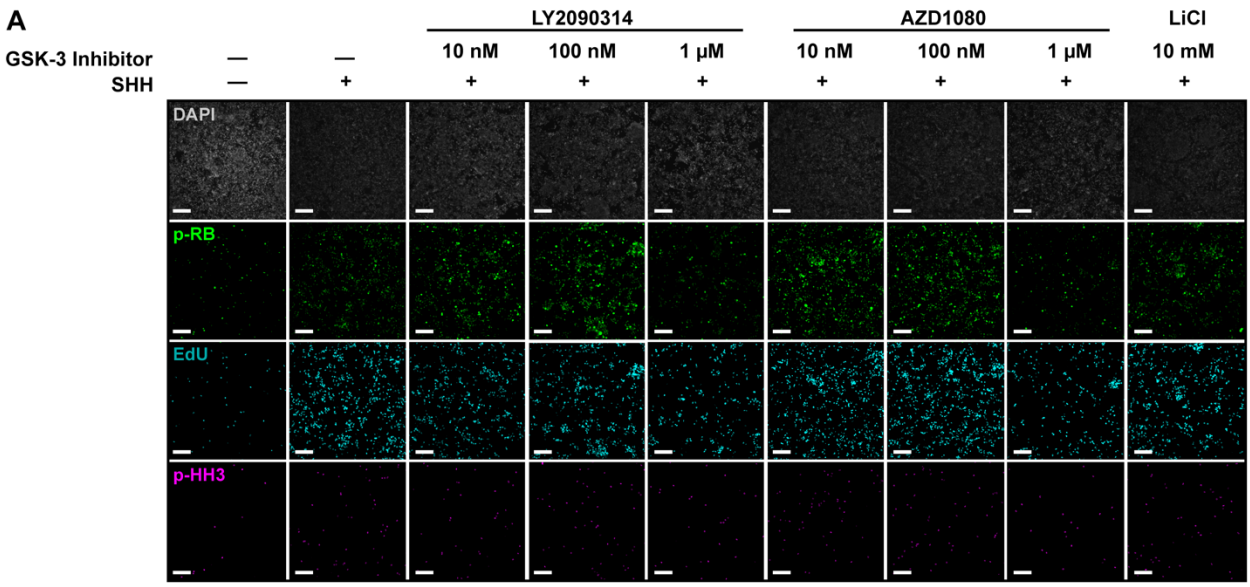

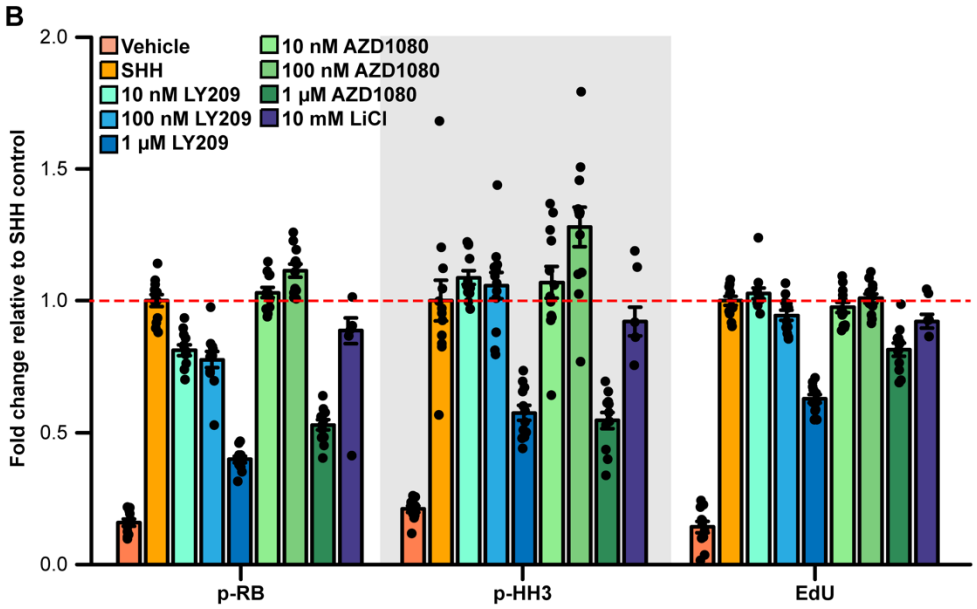

Figure S2

C

ANOVA	Condition / Marker	Controls		LY2090314			AZD1080			LiCl
		Vehicle	SHH	10 nM	100 nM	1 μM	10 nM	100 nM	1 μM	10 mM
Vehicle	p-RB	–	$< 3.1 \times 10^{-10}$	$< 3.1 \times 10^{-10}$	$< 3.1 \times 10^{-10}$	1.5×10^{-7}	$< 3.1 \times 10^{-10}$	$< 3.1 \times 10^{-10}$	$< 3.1 \times 10^{-10}$	$< 3.1 \times 10^{-10}$
	p-HH3	–	$< 3.1 \times 10^{-10}$	$< 3.1 \times 10^{-10}$	$< 3.1 \times 10^{-10}$	$< 1.1 \times 10^{-4}$	$< 3.1 \times 10^{-10}$	$< 3.1 \times 10^{-10}$	$< 5.1 \times 10^{-4}$	$< 3.1 \times 10^{-10}$
	EdU	–	$< 3.1 \times 10^{-10}$	$< 3.1 \times 10^{-10}$	$< 3.1 \times 10^{-10}$	$< 3.1 \times 10^{-10}$	$< 3.1 \times 10^{-10}$	$< 3.1 \times 10^{-10}$	$< 3.1 \times 10^{-10}$	$< 3.1 \times 10^{-10}$
SHH	p-RB	$< 3.1 \times 10^{-10}$	–	3.9×10^{-5}	5.8×10^{-7}	$< 3.1 \times 10^{-10}$	0.995	0.0553	$< 3.1 \times 10^{-10}$	0.0549
	p-HH3	$< 3.1 \times 10^{-10}$	–	0.953	0.997	1.9×10^{-6}	0.988	5.8×10^{-3}	3.2×10^{-7}	0.975
	EdU	$< 3.1 \times 10^{-10}$	–	0.988	0.626	$< 3.1 \times 10^{-10}$	0.994	0.999	2.5×10^{-7}	0.165

Tukey HSD post-hoc adjusted p-values

p-value:
n.s.
< 0.05
< 0.01
< 0.001

Fig. S2. GSK-3 inhibitors decrease proliferation in cultured CGNPs. (A) DAPI, EdU, p-RB and p-HH3 immunofluorescence images of cultured CGNPs treated with vehicle, SHH, or SHH with the indicated doses of the GSK-3 inhibitors LY2090314, AZD1080, or LiCl. CGNPs were pulse-labeled with EdU 1hr. before fixation. **(B)** Quantification of replicate cultures from **(A)** with the proportion of positive cells expressed as fold change relative to SHH controls (n=12 per condition). Error bars represent SEM. Dots represent replicate samples. **(C)**

Adjusted p-values for comparisons of vehicle-treated and SHH-treated controls to CGNPs with the indicated doses of LY209, AZD1080, or LiCl. Significance is denoted by colored boxes indicated in the legend, as determined by ANOVA with Tukey HSD post-hoc test. Scale bars measure 50 μm.

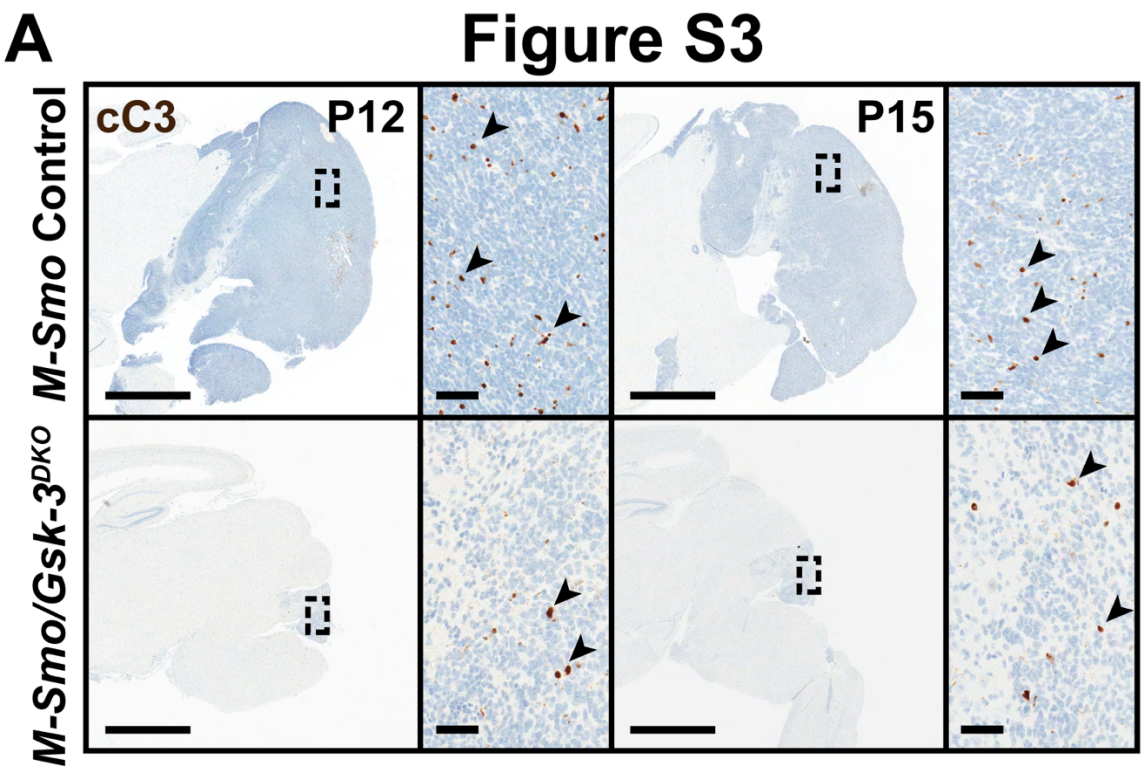

Fig. S3. *Gsk-3* deletion does not induce apoptosis in medulloblastoma-prone mice. (A) Representative sagittal sections of *M-Smo* control and *M-Smo/Gsk-3*^{DKO} mice subjected to cC3 immunohistochemistry. Black arrowheads highlight cC3^{+} cells. Scale bars measure 2 mm for low magnification images and 50 µm for higher magnification images. The regions of the higher magnification images are outlined by rectangles on the low magnification images.

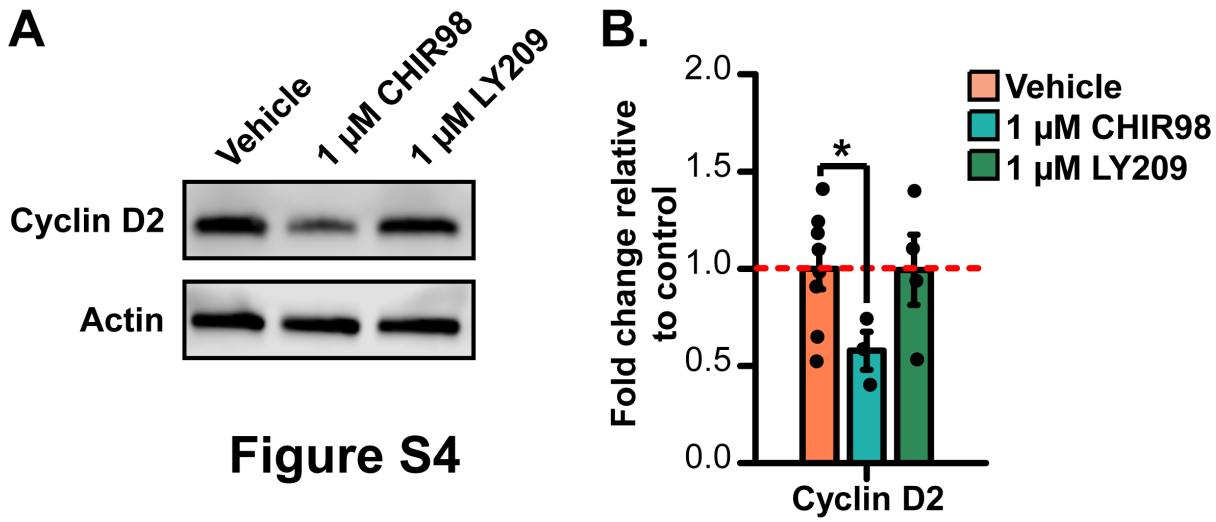

Figure S4

Fig. S4. CHIR98 decreases cyclin D2 levels in cultured medulloblastoma cells. (A) Representative western blot image comparing cyclin D2 and actin protein expression of medulloblastoma cells treated *in vitro* with vehicle, 1 μM CHIR98, or 1 μM LY209. **(B)** Quantification of replicate cultures from **(A)** with luminescence normalized to actin and expressed as fold change relative to control tumor cells (vehicle: n=8; CHIR98: n=3; LY209: n=4). Error bars indicate SEM. Dots represent replicate mice. Significance is denoted by *p<0.05, **p<0.01, ***p<0.001 as determined by student's t-test.

Table S1. The set of genes differentially expressed in whole cerebella of *Gsk-3*^{DKO} mice at P1, compared to two different, age-matched control groups, *M-Cre/Gsk-3α*$^{+/-}$*/Gsk-3β*$^{loxP/loxP}$, which retain a single *Gsk-3α* allele but have no *Gsk-3β* alleles in CGNPs, and *No Cre/Gsk-3α*$^{+/-}$*/Gsk-3β*$^{loxP/+}$, which retain a single *Gsk-3α* allele and retain two *Gsk-3β* alleles in CGNPs. Listed below are the gene names for 68 genes that were differentially expressed in the *Gsk-3*^{DKO} cerebella compared to both controls, with false discovery rate (FDR) adjusted p-value (q-value) less than 0.05 and absolute fold change (|FC|) greater than or equal to 2. The listed fold changes and p values are from the pairwise comparison of *Gsk-3*^{DKO} cerebella versus *M-Cre/Gsk-3α*$^{+/-}$*/Gsk-3β*$^{loxP/loxP}$ controls.

Gene	fold_change	FDR adjusted p_value
Chrnb4	-3.56487	4.62E-07
Mfap4	-2.77489	5.34E-08
Chrna3	-2.54283	4.04E-07
Gsk3a	-2.53513	2.76E-10
Rnf148	-2.39022	9.31E-06
Nhlh1	-2.27388	1.64E-06
Cadps2	-2.21815	1.25E-06
Pisd-ps3	-2.15748	0.0263872
A930017K11Rik	-2.15248	2.42E-05
Gm10002	-2.12494	0.031835
Gm10002	-2.12494	0.031835
Slc22a6	-2.07768	0.0109233
Esd	-2.06687	0.0235768
Gm16169	-2.00995	8.85E-05
6430573F11Rik	2.00458	8.99E-08
LOC100503213	2.01892	0.0340935
Bmp4	2.06115	0.0127298
Gna14	2.08821	3.35E-08
Gm11744	2.09393	2.32E-05
Cbln4	2.12643	0.0210509
Hoxb9	2.12871	0.00380108
Nkd1	2.15054	2.14E-05
Mettl7a2	2.21692	1.65E-06
Lrrc26	2.22882	0.000573276
Lrrc55	2.24894	2.25E-05
Igk	2.26064	0.01754
Adamts19	2.29237	5.60E-07
Cdkn1a	2.32177	7.58E-09
Dock5	2.32746	6.89E-08
Glra1	2.33206	0.00218635
Gadd45g	2.34539	3.03E-06
Axin2	2.36502	1.23E-09
Dlx3	2.3702	7.96E-09
Gpr50	2.49813	0.00257124
Syk	2.49831	2.43E-05
2700046A07Rik	2.53502	7.68E-07
Wnt10a	2.53589	2.42E-05
Tcf7	2.54261	1.17E-08

Spo11	2.65145	4.61E-06
Gadd45a	2.67878	8.94E-05
Mylk	2.6964	1.71E-05
Mafb	2.73824	6.74E-05
Gm9926	2.82476	3.98E-05
Emilin3	2.87132	3.17E-06
Rasl11b	2.87278	1.35E-06
Zfp503	2.89595	2.29E-06
C030034L19Rik	3.00969	3.49E-07
Sp5	3.15039	3.47E-07
Fzd10	3.25743	1.74E-05
Sostdc1	3.3585	2.08E-05
Ascl4	3.48996	4.28E-08
Il6ra	3.52424	1.13E-05
Lef1	3.5281	1.51E-08
Onecut1	3.59348	8.25E-06
D630039A03Rik	3.65652	8.58E-08
Gabra6	3.72096	5.96E-07
Ism1	3.81828	1.31E-06
Myo1e	3.98353	1.58E-08
Lgr6	5.12478	9.71E-08
Esyt3	5.60377	6.02E-08
Fst	5.60408	1.51E-10
Adam18	5.75826	3.27E-06
Notum	6.26911	6.56E-11
Cryba2	7.95998	3.34E-07
Mybpc1	8.1496	1.17E-09
Pmaip1	9.39472	6.77E-09
Igk	11.0986	1.10E-05
Wif1	13.0107	1.91E-11

Table S2. Materials.

Listed below are all animals, reagents, kits and other materials used, with information on source and concentration, where appropriate.

Reagent	Concentration	Source	Identifier
Animal Studies			
C57BL/6 mice	N/A	The Jackson Laboratory	Stock #000664
Math1-Cre mice	N/A	The Jackson Laboratory	Stock #011104
Gsk-3α$^{-/-}$ mice	N/A	Donated by Dr. William Snider's lab	N/A
Gsk-3β$^{loxP/loxP}$ mice	N/A	The Jackson Laboratory	Stock #029592
SmoM2-eYFP$^{loxP/loxP}$ mice	N/A	The Jackson Laboratory	Stock #005130
Trp53$^{loxP/loxP}$ mice	N/A	The Jackson Laboratory	Stock #008462
Ctnnb$^{loxP/loxP}$ mice	N/A	The Jackson Laboratory	Stock #004152
Cdkn1a$^{-/-}$ mice	N/A	The Jackson Laboratory	Stock #016565
Isoflurane	Vapor	Piramal Critical Care, Inc.	NCD Code #66794-017-25
5-bromo-2-deoxyuridine (BrdU)	100 mg/kg in 25 µl of HBSS	ThermoFisher Scientific	Catalog #B23151
5-ethnynyl-2'-deoxyuridine (EdU)	40 mg/kg in 25 µl of HBSS	Life Technologies	Catalog #A10044
PCR			
Tail lysis buffer	1X	Allele Biotechnology	Catalog #ABP-PP-MT01
Cre Forward Primer: GCG GTC TGG CAG TAA AAA CTA TC	200 µM	Invitrogen	JAX #oIMR1084
Cre Reverse Primer: GTG AAA CAG CAT TGC TGT CAC TT	200 µM	Invitrogen	JAX #oIMR1085
Gsk-3α Forward Primer: CCC CCA CCA AGT GAT TTC ACT GCT A	200 µM	Invitrogen	N/A
Gsk-3α Reverse Primer: AAC ATG AAA TTC CGG GCT CCA ACT CTA T	200 µM	Invitrogen	N/A
Gsk-3β Forward Primer: GCC ATC AAG AAA GTT CTA CAG GA	200 µM	Invitrogen	JAX #32390
Gsk-3β Reverse Primer: GCT GAA GTC CAG AGC AAG TCT	200 µM	Invitrogen	JAX #32391

Trp53 Forward Primer: GGT TAA ACC CAG CTT GAC CA	200 µM	Invitrogen	JAX #oIMR8543
Trp53 Reverse Primer: GGA GGC AGA GAC AGT TGG AG	200 µM	Invitrogen	JAX #oIMR8544
Ctnnb Forward Primer: AAG GTA GAG TGA TGA AAG TTG TT	200 µM	Invitrogen	JAX #oIMR1512
Ctnnb Reverse Primer: CAC CAT GTC CTC TGT CTA TTC	200 µM	Invitrogen	JAX #oIMR1513
Cdkn1a 1 Primer: GTT GTC CTC GCC CTC ATC TA	200 µM	Invitrogen	JAX #12427
Cdkn1a 2 Primer: GCC TAT GTT GGG AAA CCA GA	200 µM	Invitrogen	JAX #12428
Cdkn1a 3 Primer: CTG TCC ATC TGC ACG AGA CTA	200 µM	Invitrogen	JAX #12429
SmoM2-eYFP Forward primer: AAG TTC ATC TGC ACC ACC G	400 µM	Invitrogen	JAX #oIMR0872
SmoM2-eYFP Reverse primer: TCC TTG AAG AAG ATG GTG CG	400 µM	Invitrogen	JAX #oIMR1416
Apex Taq DNA Polymerase Master Mix	1X	Genessee Scientific	Catalog #42-138
Platinum Blue PCR SuperMix	1X	Invitrogen	Catalog # 12580015
Dissociation			
Papain Dissociation System	Per manufacturer's instructions	Worthington Biochemical Corporation	Catalog #LK003150
Heat inactivated FBS	100% for dissociation 10% in media	Gibco	Catalog #10437028
Hank's Balanced Salt Solution	1X	Gibco	Catalog #14175-095
D-(+)-Glucose	6g/L (33 mM)	Millipore Sigma	Catalog #G7021
Cell Culture			
Poly-L-Lysine	1X	Sigma-Aldrich	Catalog #P4832
DMEM/F12	1X	Gibco	Catalog #11330-032
N2 Supplement	1:10000 in media	BD Biosciences	Catalog #35-100
Penicillin-Streptomycin	1:10000 in media	Sigma-Aldrich	Catalog #P4333
Potassium Chloride (KCl)	2.5 µM	Mallinckrodt	Catalog #6858
Sonic hedgehog (SHH)	0.5 mg/mL	R&D Systems	Catalog #464SH
Paraformaldehyde (PFA)	4% fixative 0.1% in sheath fluid	Sigma-Aldrich	Catalog #P6148
Immunofluorescence and Western Blot			

Antigen Retrieval	1:100	Vector Laboratories	Catalog #H-3300
Phosphate Buffered Saline (PBS)	1X	Corning Inc.	Supplier #46-013-CM
Tween 20	0.3% in PBS	Sigma-Aldrich	Catalog #P9416
Donkey serum	2% in 0.3% PBST	Millipore Sigma	Catalog #D9663
Tris Buffered Saline with Tween (TBST)	1X	Cell Signaling Technology	Catalog #9997
Bovine Serum Albumin (BSA)	1% in 0.1% or 0.3% PBST	Fisher Scientific	Catalog #BP9700-100
Bicinchoninic acid (BCA) assay	Per manufacturer's instructions	Thermo Fisher Scientific	Catalog #23229
4-20% Mini-PROTEAN® TGX™ Precast Protein Gels	N/A	Bio Rad	Catalog #4561094
DAPI	1:2500 for IF	Invitrogen	Catalog #D1306
cleaved Caspase-3 (Asp175)	1:200 for IHC	Cell Signaling Technology	Catalog #9661
GSK-3α/β (D75D3)	1:100 for IF	Cell Signaling Technology	Catalog #5676
PCNA	1:2000 for IF	Abcam	Catalog #ab92552
CDKN1B/p27	1:1000	Cell Signaling Technology	Catalog #3686
phospho-RB (Ser807/811)	1:3000 for IF 1:500 for WB	Cell Signaling Technology	Catalog #8516
phospho-Histone H3 (Ser10) (6G3)	1:100 for IHC	Cell Signaling Technology	Catalog #9706
LEF1	1:200 for IF	Sigma	Catalog #HPA002087
TCF1 (C63D9)	1:100 for IF	Cell Signaling Technology	Catalog #2203
CDKN1A/p21	1:500 for WB 1:2000 for IHC	Abcam	Catalog #ab109199
phospho-CTNNB (Ser33/37/Thr41)	1:500 for WB	Cell Signaling Technology	Catalog #9561
CTNNB	1:500 for WB	Cell Signaling Technology	Catalog #8480
phospho-GSK-3β (Ser9) (D85E12)	1:500 for WB	Cell Signaling Technology	Catalog #5558
Cyclin D2 (D52F9)	1:500 for WB	Cell Signaling Technology	Catalog #3741
β-Actin (8H10D10)	1:5000 for WB	Cell Signaling Technology	Catalog #3700
Goat anti-rabbit Alexa Fluor 488	1:400 for IF	ThermoFisher Scientific	Catalog #A-11034
Goat anti-mouse Alexa Fluor 555	1:400 for IF	ThermoFisher Scientific	Catalog #A-21424

Novolink Polymer	Per manufacturer's instructions	Leica Biosystems	Catalog #RE7200-CE
ImmPRESS™ HRP Anti-Rabbit IgG	Per manufacturer's instructions	Vector Laboratories	Catalog #MP-7401
ImmPRESS™ HRP Anti-Mouse IgG	Per manufacturer's instructions	Vector Laboratories	Catalog #MP-7402
Anti-mouse IgG, HRP-linked Antibody	1.5:1000 for WB	Cell Signaling Technology	Catalog #7076
Anti-rabbit IgG, HRP-linked Antibody	1.5:1000 for WB	Cell Signaling Technology	Catalog #7074
Click-iT™ EdU Cell Proliferation Kit for Imaging, Alexa Fluor™ 488	Per manufacturer's instructions	ThermoFisher Scientific	Catalog #C10337
SuperSignal West Femto Maximum Sensitivity Substrate	Per manufacturer's instructions	Thermo Fisher Scientific	Catalog #34095
Pharmacological Inhibition			
CHIR-98014	As indicated	Selleckchem	Catalog #S2745
LY2090314	As indicated	Selleckchem	Catalog #S7063
AZD1080	As indicated	Selleckchem	Catalog #S7145
Lithium Chloride (LiCl)	As indicated	Sigma Aldrich	Catalog #203637
Flow Cytometry			
FIX & PERM Cell Fixation & Cell Permeabilization Kit	Per manufacturer's instructions	ThermoFisher Scientific	Catalog #GAS003
Heat inactivated FBS	5% in FACS wash buffer	Gibco	Catalog #10437028
Sodium azide (NaN_3)	0.1% in FACS wash buffer	Fisher Scientific	Catalog #S2271-25
FxCycle Violet	1:100	ThermoFisher Scientific	Catalog #F10347
phospho-RB Alexa Fluor 488	1:50	Cell Signaling Technology	Catalog #4277